Circulation

ORIGINAL RESEARCH ARTICLE

Extracellular Vesicle–Encapsulated Adeno-Associated Viruses for Therapeutic Gene Delivery to the Heart

Xisheng Li, PhD*; Sabrina La Salvia, PhD*; Yaxuan Liang, PhD*; Marta Adamiak, PhD; Erik Kohlbrenner, BS; Dongtak Jeong, PhD; Elena Chepurko, PhD; Delaine Ceholski, PhD; Estrella Lopez-Gordo, PhD; Seonghun Yoon, PhD; Prabhu Mathiyalagan, PhD; Neha Agarwal, MS; Divya Jha, PhD; Shweta Lodha, BS; George Daaboul, PhD; Anh Phan, PhD; Nikhil Raisinghani, MD; Shihong Zhang, BS; Lior Zangi, PhD; Edgar Gonzalez-Kozlova, PhD; Nicole Dubois, PhD; Navneet Dogra, PhD; Roger J. Hajjar, MD; Susmita Sahoo, PhD

BACKGROUND: Adeno-associated virus (AAV) has emerged as one of the best tools for cardiac gene delivery due to its cardiotropism, long-term expression, and safety. However, a significant challenge to its successful clinical use is preexisting neutralizing antibodies (NAbs), which bind to free AAVs, prevent efficient gene transduction, and reduce or negate therapeutic effects. Here we describe extracellular vesicle–encapsulated AAVs (EV-AAVs), secreted naturally by AAV-producing cells, as a superior cardiac gene delivery vector that delivers more genes and offers higher NAb resistance.

METHODS: We developed a 2-step density-gradient ultracentrifugation method to isolate highly purified EV-AAVs. We compared the gene delivery and therapeutic efficacy of EV-AAVs with an equal titer of free AAVs in the presence of NAbs, both in vitro and in vivo. In addition, we investigated the mechanism of EV-AAV uptake in human left ventricular and human induced pluripotent stem cell-derived cardiomyocytes in vitro and mouse models in vivo using a combination of biochemical techniques, flow cytometry, and immunofluorescence imaging.

RESULTS: Using cardiotropic AAV serotypes 6 and 9 and several reporter constructs, we demonstrated that EV-AAVs deliver significantly higher quantities of genes than AAVs in the presence of NAbs, both to human left ventricular and human induced pluripotent stem cell-derived cardiomyocytes in vitro and to mouse hearts in vivo. Intramyocardial delivery of EV-AAV9–sarcoplasmic reticulum calcium ATPase 2a to infarcted hearts in preimmunized mice significantly improved ejection fraction and fractional shortening compared with AAV9–sarcoplasmic reticulum calcium ATPase 2a delivery. These data validated NAb evasion by and therapeutic efficacy of EV-AAV9 vectors. Trafficking studies using human induced pluripotent stem cell–derived cells in vitro and mouse hearts in vivo showed significantly higher expression of EV-AAV6/9–delivered genes in cardiomyocytes compared with noncardiomyocytes, even with comparable cellular uptake. Using cellular subfraction analyses and pH-sensitive dyes, we discovered that EV-AAVs were internalized into acidic endosomal compartments of cardiomyocytes for releasing and acidifying AAVs for their nuclear uptake.

CONCLUSIONS: Together, using 5 different in vitro and in vivo model systems, we demonstrate significantly higher potency and therapeutic efficacy of EV-AAV vectors compared with free AAVs in the presence of NAbs. These results establish the potential of EV-AAV vectors as a gene delivery tool to treat heart failure.

Key Words: extracellular vesicles ■ genetic therapy

Gene therapy represents a major shift in medicine, with treatments for >40 diseases undergoing clinical trials,[1] and 5 US Food and Drug Administration–approved viral vector–based drugs are currently in use.[2] The gene therapy–based clinical trials include not only rare monogenic conditions such as inherited

Correspondence to: Susmita Sahoo, PhD, One Gustave L. Levy Place, Box 1030, New York, NY 10029-6574, Email susmita.sahoo@mssm.edu; or Roger Hajjar, MD, Gene & Cell Therapy Institute, Mass General Brigham, 65 Landsdowne St, Suite 143, Cambridge, MA 02139, Email Rhajjar@partners.org

*X. Li, S. La Salvia, and Y. Liang contributed equally.

Supplemental Material, the podcast, and transcript are available with this article at https://www.ahajournals.org/doi/suppl/10.1161/CIRCULATIONAHA.122.063759.

For Sources of Funding and Disclosures, see page 422.

Circulation is available at www.ahajournals.org/journal/circ

Clinical Perspective

What Is New?

- Extracellular vesicle–encapsulated adeno-associated viruses (EV-AAVs) shield AAVs from neutralizing antibodies (NAbs) and can overcome a key roadblock associated with AAV-mediated gene therapy.
- EV-AAVs are a superior cardiac gene delivery vector that offers higher NAb resistance and delivers more genes in the presence of NAbs compared with AAVs.
- EV-AAVs are cardiotropic and efficiently transduce genes to cardiomyocytes in the left ventricle for a long-term gene delivery to the heart.

What Are the Clinical Implications?

- SERCA2a gene delivered with EV-AAVs improves cardiac remodeling and function in mice with infarcted hearts even in the presence of neutralizing antibodies.
- EV-AAVs improve existing cardiac gene therapy by circumventing NAb neutralization, which can expand the patient population receiving gene therapy by including NAb$^+$ patients with heart failure and can enable redosing in already treated patients (with AAV gene therapy).
- EV-AAVs are a clinically compatible, next-generation cardiac delivery vector that can advance current AAV-based therapeutic applications for treating cardiovascular diseases.

Nonstandard Abbreviations and Acronyms

AAV	adeno-associated virus
AAVR	adeno-associated virus receptor
BLI	bioluminescent imaging
CLIC	clathrin-independent carrier
CM	cardiomyocyte
EF	ejection fraction
EV	extracellular vesicle
EV-AAV	extracellular vesicle–encapsulated adeno-associated virus
FS	fractional shortening
GEEC	glycosylphosphatidylinositol-anchored protein-enriched endosomal compartment
hiPSC	human induced pluripotent stem cell
MI	myocardial infarction
NAb	neutralizing antibody
NM	noncardiomyocyte
qPCR	quantitative polymerase chain reaction
SERCA2a	sarcoplasmic reticulum calcium ATPase 2a
TEM	transmission electron microscopy
TGN	trans-Golgi network
WT	wild-type

cardiomyopathies[3–5] but also more common ones like diabetes and heart failure.[6–8] Available pharmacological drugs to treat heart failure control the symptoms and the disease but do not cure it. In contrast, gene therapy has the potential to correct underlying defects and pathologies and to mediate long-lasting improvements in cardiomyocyte (CM) function.[9–11] Current strategies for myocardial gene transfer use adeno-associated viruses (AAVs) due to their nonpathogenic capacity,[1] rare integration,[12–14] and prolonged, high transgene expression level.[15–17] Recombinant AAV serotypes (called AAVs) have been shown to persist largely as episomes for ≈24 months after transduction,[18] a result that shows that AAVs are highly suitable for chronic heart failure therapy.

Although the concept of systemically delivering AAV to intervene directly within the genetic and molecular foundations of cardiac cells is simple and elegant, the path to clinical reality has been arduous. One major obstacle is the presence of neutralizing antibodies (NAbs), which form during natural exposure to AAV or after AAV administration. Data from clinical studies suggest that AAV NAbs, even at relatively low titers, block gene transduction and reduce or negate the effects of therapy.[19,20] NAbs against AAVs increase with age and appear to be common in all populations studied.[21] The high prevalence of preexisting AAV NAbs in patients hinders the efficiency of AAV-based gene therapy and limits the number of patients eligible for enrollment in gene therapy trials.[19–24] In a recent clinical study of gene therapy with AAV1/sarcoplasmic reticulum calcium ATPase 2a (AAV1/SERCA2a),[25] AAV1 NAbs were found in 59.5% of a cohort of 1552 patients with heart failure. In a separate study, high-dose immunosuppression did not prevent AAV1 NAb formation in minipigs.[25] Because patients may require >1 administration of viral-based gene therapy, strategies to circumvent NAbs are necessary.

Extracellular vesicles (EVs) are membrane-bound vesicles that actively shuttle biomolecules such as lipids, proteins, and RNA released from different cell types. Recent studies have shown that EVs encapsulate several types of viruses, including hepatitis, HIV, and AAV,[26–33] and protect these viruses from antibody-mediated neutralization. Delivering AAVs protected by carrier EVs (EV-encapsulated AAVs [EV-AAVs]) is a promising approach to circumvent NAb neutralization in AAV-based gene therapy. The robust EV membrane can shield AAVs from NAbs, and EV-AAVs can therefore present higher resistance to NAbs.[34] Current research indicates that naturally secreted large and small EVs from AAV-producing HEK293T cells can carry and deliver intact AAVs[34] to the retina,[33] inner ear,[27] liver,[3] and nervous system[28] in mice.

Free AAVs, along with EV-AAVs, are secreted out to the conditioned media of AAV-producing cells. The presence of free AAVs in EV-AAV preparations may reduce effective EV-AAV dosing, lower their NAb resistance, and cause unwanted side effects from higher levels of free AAVs. Efficiently removing free AAV contaminants from EV-AAVs is a critical first step in their clinical translation. Earlier attempts to purify EV-AAVs with neurotropic AAV serotypes 1, 8, and 6[32,35,36] resulted in limited NAb resistance, possibly due to insufficient separation from AAVs or their inadequate characterization. Here, we evaluated the delivery and therapeutic efficacy of EV-AAV–mediated gene transfer to the heart compared with methods that use standard free AAV vectors, both with and without NAbs. We: (1) optimized an ultracentrifugation-based EV-AAV purification strategy to isolate highly pure EV-AAVs from conditioned medium from AAV-producing HEK293T cells, with minimum free AAV contamination; (2) comprehensively characterized EV-AAV size, purity, concentration, morphology, presence of EV marker proteins, and molecular content; (3) evaluated the gene delivery efficacy and NAb resistance of EV-AAVs compared with standard free AAV vectors using cardiotropic AAV serotypes 6 and 9 and several reporter constructs in both human left ventricular CMs and human induced pluripotent stem cell (hiPSC)–derived CMs in vitro and in murine hearts in vivo; (4) validated the therapeutic efficacy of EV-AAV–mediated delivery compared with AAV-mediated delivery of SERCA2a in a preclinical model of myocardial infarction (MI) in preimmunized mice; and (5) investigated EV-AAV intracellular trafficking and cardiotropic mechanisms in mice hearts in vivo and human CMs in vitro. Together, with the use of 5 different in vitro and in vivo model systems, our findings established a new strategy for clinical translation of AAV-based cardiac gene therapy.

METHODS

The data that support the findings of this study are available from the corresponding author on reasonable request. Expanded methods are provided in the Supplemental Material.

Study Design

The aim of our study was to evaluate the efficacy of EV-AAVs for cardiac gene delivery and NAb resistance. First, we designed a 2-step iodixanol density-gradient ultracentrifugation method to purify EV-AAVs free of AAV contamination. We comprehensively characterized the isolated EV-AAVs for their morphology, presence of EV-specific markers, size, concentration, and AAV genome titer using Western blot, nano-flow cytometry, tunable resistive pulse sensing with qNano, quantitative polymerase chain reaction (qPCR), transmission electron microscopy (TEM), dynamic light scattering analysis, ExoView chip analysis, and RNA sequencing. Next, we designed in vitro and in vivo studies using 5 different model systems, cardiotropic AAV serotypes 6 and 9, and several reporter constructs to evaluate the gene delivery efficacy of EV-AAVs in the presence of NAb and compared them with free AAVs. We used flow cytometry, confocal microscopy, and in vivo bioluminescence imaging to quantify gene delivery and gene expression. To assess the therapeutic potential of EV-AAVs, we intramyocardially injected EV-AAV9–SERCA2a to post-MI (ligation of left anterior descending artery) mouse hearts with or without NAb and evaluated percentage of ejection fraction (EF) and percentage of fractional shortening (FS) of the heart by echocardiography. To investigate the mechanism of EV-AAV uptake in CMs, PKH67-fluorescent dye or pH-sensitive (CypHer) dye-labeled EV-AAVs were used to quantify internalization of EV-AAVs in vivo or in vitro using flow cytometry and immunofluorescence. All animal procedures were approved by the Icahn School of Medicine at Mount Sinai animal care and use committee. Nude mice (Nu/J; ≈8–10 weeks of age) were used in all our studies.

Statistical Analysis

Groups were first assessed for normality to determine whether parametric or nonparametric tests would be used. Assumptions of normality were tested with Shapiro-Wilk test. The Levene test was used for equality of variances. Normally distributed data with equal variances were statistically analyzed with either 2-tailed Student *t* test (2 groups) or 1-way ANOVA (≥3 groups with 1 experimental factor) with Tukey multiple-comparison test. Normally distributed data with unequal variance were statistically tested with either the Welch *t* test (2 groups) or Welch 1-way ANOVA (≥3 groups with 1 experimental factor), followed by the Dunnett-T3 multiple-comparison test. Normally distributed data with 2 experimental factors were analyzed with 2-way ANOVA followed by pairwise comparisons with Bonferroni multiple-comparison test or Dunnett multiple-comparison test. Repeated-measures data with 2 experimental factors were analyzed with 2-way repeated-measures ANOVA followed by the Bonferroni multiple-comparison test. For not normally distributed data, the Mann-Whitney *U* test was used to compare 2 groups. All data are shown as either the mean±SEM (normally distributed data) or median±range or interquartile range (not normally distributed data). All data were graphed by Prism 9 (GraphPad software, version 9.5.0), and statistical analyses were performed in SPSS (IBM SPSS Statistics, version 29.0). The statistical details, sample size, and significance levels for each experiment are specified in the figure legends.

RESULTS

Density Gradient Ultracentrifugation Purification Successfully Enriched EV-AAVs

Our overall goals were to isolate and thoroughly characterize highly purified EV-AAVs and to evaluate its cardiac gene delivery efficacy and NAb resistance compared with conventionally produced free AAVs (Figure 1A). US Food and Drug Administration–approved HEK293T cells, widely used to generate AAVs, are known to secrete EVs.[37–39] Several previous studies have demonstrated that AAV-producing HEK293T cells naturally secrete EV-AAVs into cell culture media.[28,29,35] To determine

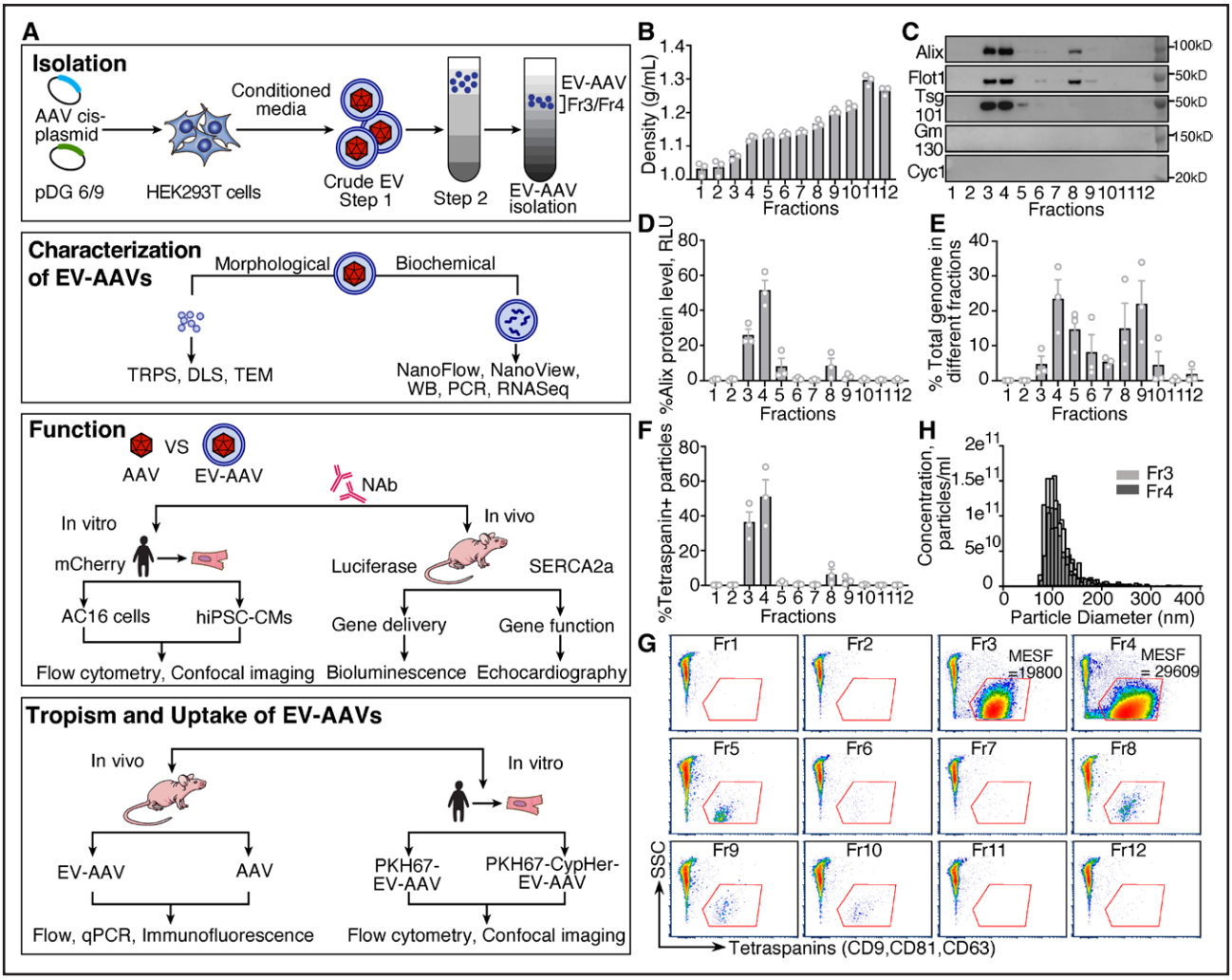

Figure 1. Density-gradient ultracentrifugation-based purification process successfully enriched EV-AAVs.
A, Schematic of extracellular vesicle–encapsulated adeno-associated virus (EV-AAV) isolation, characterization, function, tropism, and uptake mechanism. **B**, Density of 12 fractions obtained after iodixanol density-gradient ultracentrifugation (n=3). **C**, Western blot analysis of the 12 fractions. Equal volume of fractions was loaded on SDS-PAGE gels, and membranes were blotted with Alix, Flot1, Tsg101, Gm130, and Cyc1. **D**, Western blot quantification for the percent of Alix-relative expression in 12 fractions (n=3). **E**, Determination of AAV vector genomes with quantitative polymerase chain reaction in the 12 fractions (n=3). **F** and **G**, Nano-flow cytometry analysis and quantification of surface tetraspanin proteins, including CD63, CD81, and CD9, in the 12 fractions (n=3). Mean equivalent soluble fluorochromes (MESFs) were used to calibrate the fluorescence scale in MESF units for each fraction. No MESF values were detected in fractions other than Fr3 and Fr4, in which EV-AAVs were properly separated from other contaminants. **H**, Tunable resistive pulse sensing (TRPS)–qNano analysis of Fr3 and Fr4 measured EV-AAV size. Values in **B** and **D** through **F** are presented as mean±SEM.

the AAV-secretory potency of AAV-producing HEK293T cells, we quantified the total amounts of AAVs (EV-AAVs and free AAVs) either secreted into conditioned media or contained within the cells (Figure S1A). We found modest variations in AAV-secretory potency by serotype (AAV6 and AAV9; Figure S1B), in line with recently published literature.[39]

To optimize EV-AAV yield and to minimize free AAV presence, we meticulously designed a sequence of steps. Beginning with conditioned media from AAV-producing HEK293T cells (Figure S2), our step 1 involved sequential centrifugation and ultracentrifugation resulting in crude EV-AAV pellets potentially containing free AAV capsids and other contaminants (Figure S2). A control experiment using standard free AAVs revealed that these crude pellets may pull down different quantities (>80% of the starting amount) of free AAVs after step 1 (Figure S3A). Because the presence of free AAV in EV-AAV preparations could decrease NAb resistance and vary dosing, we devised step 2 (Figure S2) to remove free AAVs through a modified iodixanol density gradient ultracentrifugation, with each fraction characterized thoroughly.

Density measurements of all 12 fractions (Fr) from step 2 revealed that Fr3 and Fr4 had the buoyance density reported for EVs (1.07–1.13 g/mL; Figure 1B). Western blot analysis found Fr3 and Fr4 to be positive for known EV markers Alix, Flot1, and Tsg101 and

negative for known EV negative controls Gm130 (Golgi marker) and Cyc1 (mitochondria marker; Figure 1C and 1D; Figure S4A). Fr3 and Fr4 also contained the majority of AAV vector genomes, as determined by qPCR (Fr3 and Fr4, 28±13%; Figure 1E). Meanwhile, quantification of EVs using nano-flow cytometry for surface tetraspanin markers (CD81, CD63, and CD9) and tunable resistive pulse sensing–qNano technique for total particle count showed that the majority of pure EV-AAVs are enriched in Fr3 and Fr4 (Fr3 and Fr4, 87.3±6.9% for tetraspanin-positive particles; Fr3 and Fr4, 99.7±0.2% for total particles; Figure 1F and 1G; Figure S4B). To confirm EV-AAV presence in Fr3 and Fr4, we used tunable resistive pulse sensing–qNano to measure particle size, which was found to be ≈110 nm (Figure 1H; Figure S4C and S4D). In addition, we detected a weak unreliable signal measuring size and particle concentration from Fr8 (Figure S4E; no particles were detected in Fr1, Fr2, Fr5–Fr7, and Fr9–Fr12), suggesting the presence of protein aggregations or contaminating membrane fragments/viral components in Fr8, which were heavier than EVs and difficult to dissolve. To estimate the extent of free AAVs coisolated with EV-AAVs in Fr3 and Fr4, we subjected different free AAVs doses (as a control) to step 1 and step 2 purification process identical to the EV-AAV isolation protocol. The majority (≈60%–70%) of free AAVs were found to be concentrated in Fr11 (as expected, between the 40% and 60% iodixanol solution), and negligible amounts (≈3%–5%) were found in Fr3 and Fr4 (Figure S3B). These data are consistent with our particle size, concentration, and EV marker data and confirm that our EV-AAV preparations from Fr3 and Fr4 are primarily AAV-encapsulating EVs, mostly free of contaminants such as protein aggregates, membrane fragments, and free AAVs. The low AAV levels detected in Fr11 in step 2 (Figure 1E) suggest that the majority, if not all, of AAVs secreted by the AAV-producing HEK293T cells into the conditioned media could be EV-AAVs.

Taken together, these results demonstrate that our 2-step iodixanol density-gradient ultracentrifugation protocol successfully isolated EV-AAVs in Fr3 and Fr4, which are coenriched for EV biomarkers, consistent with the density and size of EVs, and contain viral vector genomes. In our subsequent experiments, we further characterize and investigate EV-AAVs from Fr3 and Fr4 and compared their characteristics and function with free AAVs.

EV-AAVs Share Morphological and Biochemical Characteristics With Wild-Type EVs

To verify AAV presence and location in isolated EV-AAVs, we processed ultrathin sections of EV-AAV pellets and imaged them using TEM. Wild-type (WT) EVs (from untransfected HEK293T cells) and free AAVs were used as controls. TEM micrographs of EV-AAV sections show that the majority of AAVs (measuring ≈20–25 nm, consistent with known AAV sizes) in Fr3 and Fr4 EV-AAV preparations were encapsulated in membranous EVs ≈100 nm in size (white arrows in Figure 2A; Figure S5). We used dynamic light-scattering analysis to confirm the sizes of EV-AAVs, EV-WT, and free AAVs. We observed particles with sizes corresponding to EVs (≈100 nm, in line with our TEM and qNano measurements) and free AAVs (≈20 nm, similar to TEM measurements; Figure 2B). No significant size differences between EV-AAVs and EV-WT were detected. Nano-flow cytometry analysis for EV surface marker proteins showed no difference in tetraspanin expression between EV-AAVs and EV-WT (Figure 2C). In accordance with nano-flow cytometry data, ExoView Chip, an interferometry-based protein expression profiling technique, revealed canonical EV markers such as tetraspanin CD81, CD63, and CD9 on both EV-AAVs and EV-WT (Figure 2D). Expression of CD9 in EV-AAVs was significantly decreased compared with EV-WT (Figure 2E). In addition, EV-AAVs and EV-WT carried similar EV marker proteins: Alix, Tsg101, and Flot1 (Figure 2F). As expected, the viral capsid proteins VP1, VP2, and VP3 were detected in EV-AAVs and AAVs but not in EV-WT (Figure 2F). We detected stronger VP1/2/3 band intensity in EV-AAVs than free AAVs, even when equal titers of vector genomes (quantified by qPCR) were loaded (Figure 2F). To address this discrepancy and to examine viral genome integrity, we analyzed the DNA using alkaline agarose gel electrophoresis (Figure 2G) from equal titers of EV-AAVs and AAVs and quantified the DNA band intensity. There was no significant difference in DNA quantities between EV-AAVs and free AAVs (Figure 2H), confirming the accuracy of viral genome titer determination by qPCR. More VP1/2/3 protein in EV-AAV isolates may implicate the presence of higher quantities of empty capsids compared with AAVs.[40]

To identify distinct transcriptomic signatures in EV-AAVs and EV-WT, we sequenced the RNA from both using small RNA sequencing. Principal component analysis determined the axis of variance and revealed that EV-AAVs and EV-WT were enriched for both common and unique transcriptomic profiles (Figure 2I and 2J; Figure S6A–S6C). There were ≈600 common transcripts between EV-WT and EV-AAVs, whereas EV-AAVs had >200 unique transcripts, indicating that novel molecular signatures originate from AAV-transfected cells (Figure 2J). Heat map analysis showed the top differentially expressed RNAs between EV-AAV and EV-WT (Figure 2K; Figure S6D). Both EV-AAVs and EV-WT contained coding and noncoding RNAs that modulated protein stability and metabolism (Figure S6E; Table S1 and S2). However, EV-AAVs also contained unique RNA cargo that regulates cholesterol metabolism (eg, MYLIP), myosin regulation (CFAP20), growth, and differentiation factors (NRG-2), which may exert beneficial functions (Figure S7A and S7B). The RNAs unique to EV-AAVs

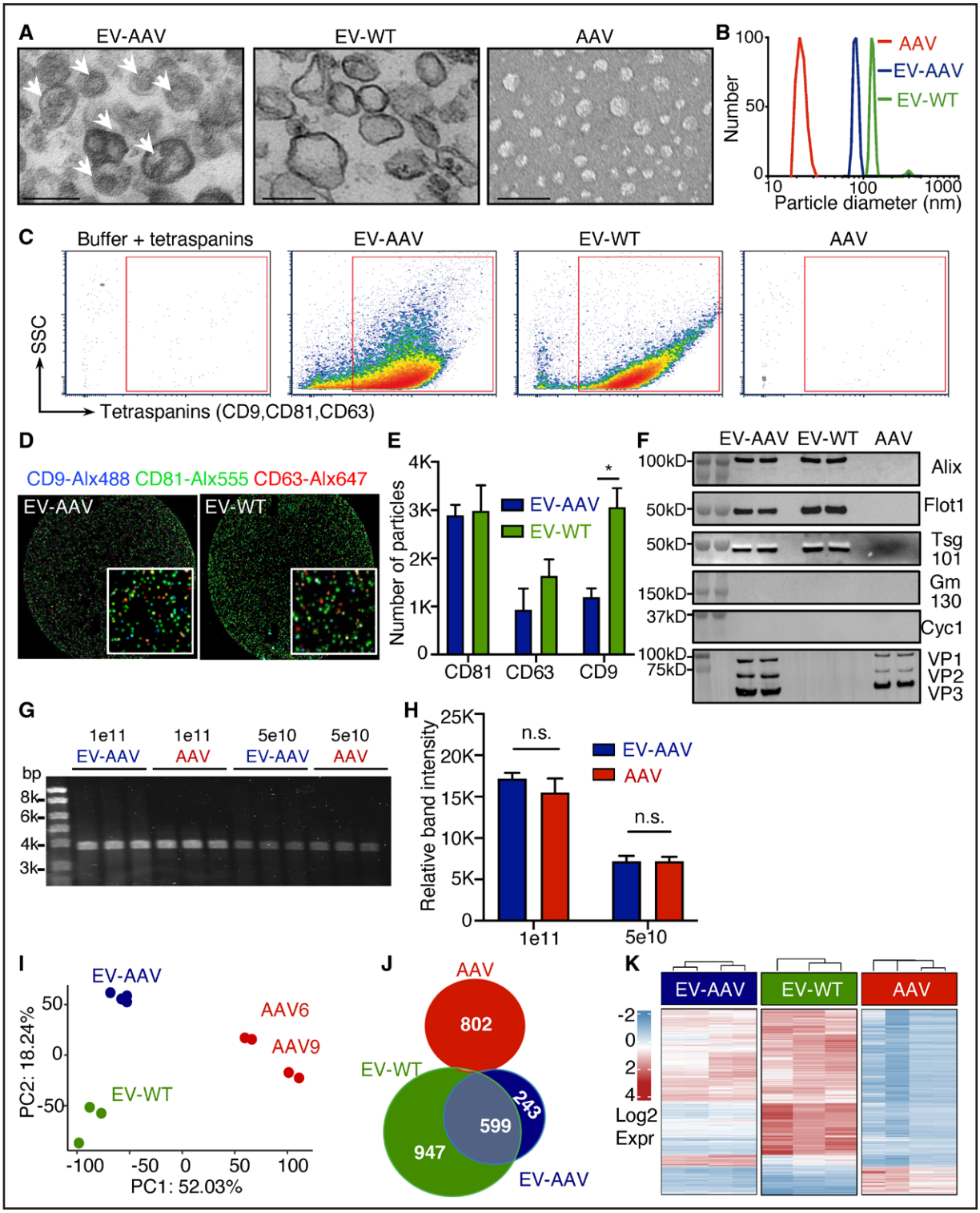

Figure 2. EV-AAVs share morphological and biochemical characteristics with EV-WT and are enriched for unique transcriptomes.

A, Representative images of transmission electron microscopy (TEM) for extracellular vesicle (EV)–encapsulated adeno-associated viruses (AAVs; **left**), wild-type EVs (EV-WT; **middle**), and free AAVs (**right**); arrows indicate virus particles inside EVs. Scale=100 nm. **B**, EV-AAV, EV-WT, and free AAV sizes measured by dynamic light scattering (DLS) analysis. **C**, Nano-flow cytometry analysis of EV-AAVs, EV-WT, and free AAVs for the presence of surface tetraspanin proteins, including CD63, CD81, and CD9. Buffer plus tetraspanin was used as a control for gating. **D** and **E**, Distribution and quantification of tetraspanin (CD63, CD81, and CD9)-positive particles in EV-AAVs and EV-WT by NanoView chips. **F**, Western blot of EV-AAVs, EV-WT, and free AAVs. Equal protein amounts (5 μg) for EV-AAV and EV-WT and equal AAV genomes (1e11 vector genomes [vg]) for EV-AAVs and free AAVs were loaded in the SDS-PAGE gel (n=2 technical replicates). Membranes were blotted with Alix, Flot1, Tsg101, Gm130, Cyc1, and VP1/VP2/VP3. **G**, Image of alkaline agarose gel electrophoresis for equal vg (1e11 and 5e10) of EV-AAVs (*Continued*)

Figure 2 Continued. and free AAVs. **H**, Quantification of band intensity of **G**. **I**, Principal component analysis to identify the axis of variance showing that EV-AAV, EV-WT, and AAV each enriched for unique transcriptomic profiles. **J**, Venn diagram showing an overlap among EV-AAV, EV-WT, and AAV and a set of common RNAs present in EV-AAV and EV-WT. **K**, Heat map with top differentially expressed profiles for EV-AAV, EV-WT, and AAV. The scale is standardized (*z* score) from the $\log_2$ expression values showing the upregulated genes in red and the downregulated genes in blue. Values in **E** and **H** were analyzed with 2-way ANOVA with Tukey multiple-comparison test. Data are presented as mean±SEM (n=3). **P*<0.05. n.s. Indicates not significant.

may augment the benefits of EV-AAV gene therapy.[41,42] We also sequenced free AAVs and FBS (2% FBS in which the HEK cells were cultured) as control samples, and as expected, neither contained significant amounts of RNA nor showed presence of identical contaminants (Figure S6B through S6D). Therefore, samples were not considered in subsequent analyses.

These results confirm that the EV-AAVs used in our subsequent studies represent AAV-carrying vesicular fractions with morphology and antigen expression similar to those of exosomes (small EVs of endocytic origin; Figure 1B through 1H). We also demonstrate that EV-AAVs and EV-WT share certain morphological and biochemical characteristics (Figure 2).

Together, our 2-step density-gradient ultracentrifugation protocol successfully isolated EV-AAVs, as determined from EV buoyance density; presence of EV surface marker proteins, viral capsid proteins, and genome; size and morphology; presence of AAVs in the lumen of EVs; and EV-AAV protein and RNA profiles. Moreover, TEM pictures of EV-AAVs, along with parallel processing of a free AAV control, established that free AAV contamination is negligible in our EV-AAV preparations. Our comprehensive characterization of EV-AAV is in line with MISEV2018 (Minimal Information for the Study of EVs) guidelines.[43]

EV-AAV Outperforms AAV in Delivering Genes to Human CMs in the Presence of NAbs In Vitro

Preexisting NAbs against AAV are prevalent in human serum.[24,44] NAbs bind to AAV, block its infection, and impair AAV-mediated gene delivery.[45–47] CMs are largely nondividing and are therefore promising targets for therapeutic AAV vectors. Recent reports have demonstrated that membrane-associated AAV vectors can very efficiently transduce various cell types and are less susceptible to antibody-mediated neutralization.[35,48,49] Thus, we hypothesized that EV-mediated AAV delivery would shield AAV vectors from preexisting humoral immune responses and thereby facilitate improved cardiac gene transfer to CMs in the presence of NAbs. To validate this, we first evaluated the transduction efficiency of EV-AAV6 encoding mCherry in human CMs in vitro. AAV6 is known to be a muscle-tropic serotype and has superior transduction efficiency in vitro.[50,51] Infecting equal titers of AAV6/9 and EV-AAV6/9 resulted in significantly higher transduction efficiency of AAV6/EV-AAV6 compared with AAV9/EV-AAV9 (Figure S8). This also confirmed that EV-AAV6 can successfully deliver genes to human left ventricular (hAC16)-CMs in vitro.

Equal titers of EV-AAV6-mCherry and free AAV6-mCherry were preincubated with NAb (0–4 mg/mL human intravenous immunoglobulins)[52] for 30 minutes at 37°C and treated to hAC16-CMs or hiPSC-CMs (Figure 3). Vector transduction efficiency was assessed by quantifying mCherry expression with flow cytometry and confocal microscopy. Our results showed significantly higher transduction efficiency by EV-AAV6 in the presence of NAb in both hAC16-CMs (Figure 3A through 3D) and SIRPA-positive hiPSC-CMs (Figure 3E through 3H; Figure S9). It is remarkable that EV-AAV6-mCherry retained significantly high transduction efficiency in both hAC16-CMs and hiPSC-CMs even at the highest concentration of NAbs (79.2±4.3% and 69.2±13.9%, respectively, at 4 mg/mL), whereas free AAV6-mCherry transduction was almost completely blocked (0.18±0.29% and 1.6±1.0%, respectively, at 4 mg/mL; Figure 3C and 3F). These results confirm that EV-AAV vectors deliver genes more effectively to CMs while also protecting the AAVs from neutralization by anti-capsid antibodies.

EV-AAV Outperforms AAV in Delivering Genes to Mouse Hearts in the Presence of NAb in Vivo

Passive-Immunity Nude Mouse Model Efficiently Mimics Naturally Occurring Immunity to AAV

To evaluate EV-AAV–mediated gene delivery and NAb resistance in vivo, we used an animal model with preexisting AAV immunity by intravenously injecting nude mice with intravenous immunoglobulins (1 mg per mouse).[30] After 24 hours, we intravenously injected the mice with an equal titer of either EV-AAV9 or AAV9 (Figure S10A). AAV9 serotype has been shown to have the highest cardiac gene transduction efficacy in rodents with either systemic or direct cardiac injection.[53] Sera isolated from intravenous immunoglobulin–preinjected mice (NAb^+) at 4 weeks significantly inhibited AAV9-FLuc (coding firefly luciferase) in vitro transduction compared with sera from saline-injected mice (NAb^-; Figure S10B). In addition, sera from NAb^+ or NAb^- mice injected with AAV or EV-AAV almost completely prevented AAV9-FLuc transduction in vitro, suggesting that administering AAV or EV-AAV stimulated the mice to produce natural antibodies that were functionally identical to the NAbs we injected (Figure S10B). In summary, we confirmed the

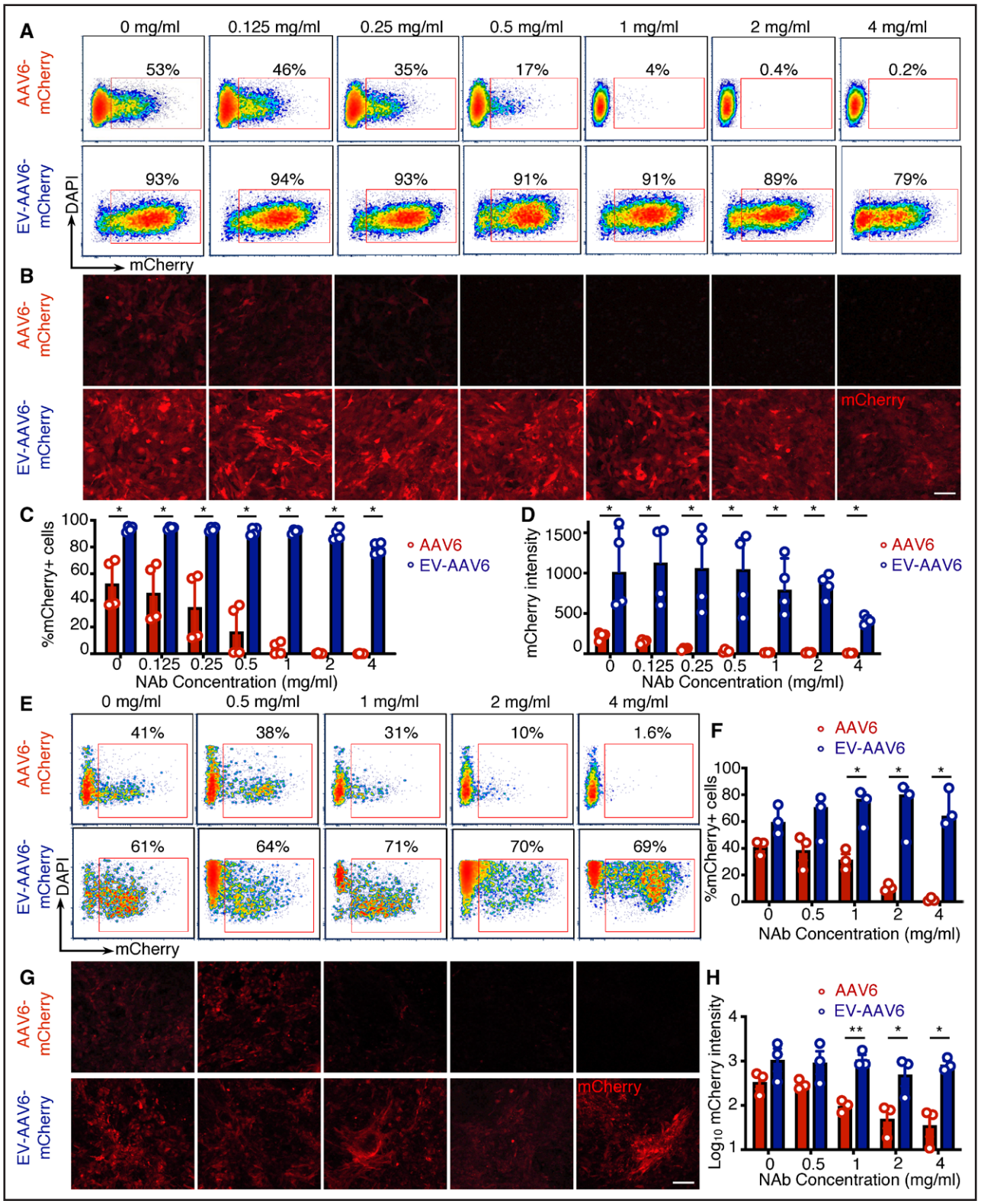

Figure 3. EV-AAVs outperform AAVs in gene delivery efficiency to human cardiomyocytes in the presence of NAb in vitro. **A** and **B**, Representative images of flow cytometry and confocal microscopy analyses of hAC16-CMs at 3 days after infection with equal titers of EV-AAV6-mCherry and AAV6-mCherry. Before being added to cell cultures, adeno-associated virus 6 (AAV6) or extracellular vesicle (EV)–encapsulated AAV6 preparations were incubated with neutralizing antibody (NAb) solution (0.125–4 mg/mL) or equal volume of PBS for 30 minutes at 37°C. Scale bar=150 μm. **C**, Flow cytometry quantification of mCherry$^+$ hAC16 cardiomyocytes (CMs) after EV-AAV6 or AAV6 transduction at different NAb concentrations (n=4). **D**, Confocal microscopy quantification of mCherry intensity in hAC16-CMs after EV-AAV6 or AAV6 transduction at different NAb concentrations (n=4). Values in **C** and **D** are presented as median with range and were (*Continued*)

Figure 3 Continued. analyzed with the Mann-Whitney *U* test (*P<0.05). **E** and **F**, Representative images of flow cytometry and confocal microscopy analyses of human induced pluripotent stem cell (hiPSC)–CMs at 3 days after infection with equal titers of EV-AAV6-mCherry and AAV6-mCherry. Before being added to cell cultures, AAV6 or EV-AAV6 preparations were incubated with NAb solution (0.5–4 mg/mL) or equal volume of PBS for 30 minutes at 37°C. Gating for mCherry$^+$ population is derived from the SIRPA (signal regulatory protein alpha)$^+$ population. Scale bar=150 μm. **G**, Flow cytometry quantification of mCherry$^+$ hiPSC-CMs after EV-AAV6 or AAV6 transduction at different NAb concentrations (n=3). **H**, Confocal microscopy analysis of mCherry intensity in hiPSC-CMs transduced with EV-AAV6 or AAV6s at different NAb concentrations (n=3). Values are presented as $\log_{10}$ mCherry fluorescent intensity. **B** and **G** were adjusted with the same brightness and contrast. Values in **F** and **H** are presented as mean±SEM and were analyzed with the Welch *t* test. *P<0.05; **P<0.01.

neutralizing effect of the sera from NAb-preinjected mice.

Empty Virus Capsids Overcome NAb-Mediated Immunity to AAV

To confirm the neutralizing effect against AAV in a preexisting NAb mouse model, we designed a NAb competition binding assay with an empty AAV capsid. Empty AAV capsids compete with AAV particles for NAb binding, thereby increasing AAV transduction in the presence of NAb. Nude mice were passively immunized with NAb 24 hours before receiving AAV9-FLuc or empty AAV9 capsids followed by AAV9-FLuc (Figure S10C). After 2 or 4 weeks, we quantified FLuc expression in these mice by bioluminescent imaging (BLI) of the chest area in vivo and isolated hearts ex vivo. AAV-mediated FLuc expression was inhibited in NAb$^+$ compared with NAb$^-$ mice (Figure S10D and S10E). Remarkably, mice injected with the same titers of both empty capsids and standard AAVs showed luciferase expression similar to NAb$^-$ mice (Figure S10D and S10E), suggesting that empty AAV capsids compete with standard AAV particles for NAb binding.

EV-AAVs Deliver Genes in the Presence of NAb

To test the gene delivery efficacy of EV-AAVs in vivo and to compare with free AAVs, nude mice were injected with NAb (NAb$^+$ mice; 1 mg per mouse) or saline (NAb$^-$ mice). After 24 hours, equal titers of EV-AAV9–FLuc or AAV9-FLuc were injected intramyocardially, and FLuc expression was quantified with BLI of live mice and of their harvested organs after death at 4 weeks (Figure 4A). Luciferase expression was higher in the EV-AAV9–FLuc–injected mice than the AAV9-FLuc–injected mice at 1 and 2 weeks (Figure S11) and both the NAb$^+$ and NAb$^-$ mice at 4 weeks (at least 2-fold; Figure 4B and 4C). In the AAV9-FLuc-NAb$^+$ mice, luciferase expression was significantly lower than in the EV-AAV9–FLuc–NAb$^+$ mice; however, there was no difference between EV-AAV9–FLuc–NAb$^-$ and EV-AAV9–FLuc–NAb$^+$ mice. These data demonstrate that EV-AAVs protect the encapsulated AAVs from NAb neutralization. Consistent with the in vivo BLI results, ex vivo imaging of isolated whole hearts showed significantly elevated luciferase expression in the EV-AAV9–FLuc–injected hearts than the AAV9-FLuc hearts in the presence of NAb (Figure 4D and 4E). We also observed similarly elevated luciferase expression in the livers of NAb$^+$ and NAb$^-$ mice treated with EV-AAV9–FLuc compared with standard AAV9-FLuc (Figure S12A and S12B), although other organs such as spleen, brain, and kidney had almost no expression (Figure S12C). Transduction was also detected in the liver but not other organs, and AAV9 vectors were consistent with the organ specificity previously described for this serotype.[54]

These data provide compelling evidence that EV-AAVs, but not free AAVs, resist neutralization by NAb in vivo in a murine model. In addition, these results demonstrate that gene delivery by EV-AAVs is significantly more effective than gene delivery by free AAVs in both the absence and presence of preexisting antibodies.

EV-AAV–Mediated SERCA2a Gene Delivery Significantly Improves Cardiac Function in the Presence of NAb in a Preclinical Mouse Model of MI

Having confirmed that EV-AAV9 vectors evade NAbs in mice, we investigated therapeutic delivery of genes such as SERCA2a to the myocardium in a preclinical setting. Earlier studies by our group and others have shown that SERCA2a plays a major role in regulating the calcium level in CMs, thereby affecting contractile function.[23,55–57] Reduced SERCA2a activity closely associates with contractile dysfunction and heart failure.[58,59] Specifically, our previously published studies showed that AAV-mediated SERCA2a gene delivery reversed contractile dysfunction and myocardial remodeling in both rodent[60,61] and large-animal models.[62] However, NAb prevalence is still a significant obstacle to delivering genes[21,25] such as SERCA2a to patients.

To address this challenge, we compared the therapeutic effect on cardiac function of SERCA2a delivered with EV-AAV9 versus free AAV9 in an MI model in nude NAb$^-$ and NAb$^+$ mice. MI was induced in mice by permanent ligation of the left anterior descending artery 24 hours after injection of either NAb or saline. Immediately after MI surgery, NAb$^+$ and NAb$^-$ mice were injected intramyocardially with an equivalent vector dose of either EV-AAV9–SERCA2a or AAV9-SERCA2a (1e11 vector genomes per mouse). To test functional improvements, cardiac EF and FS were evaluated by echocardiography 2, 4, and 6 weeks after surgery (Figure 5A). At the 6-week follow-up, EF was significantly higher in the NAb$^-$ mice that received EV-AAV9–SERCA2a than in

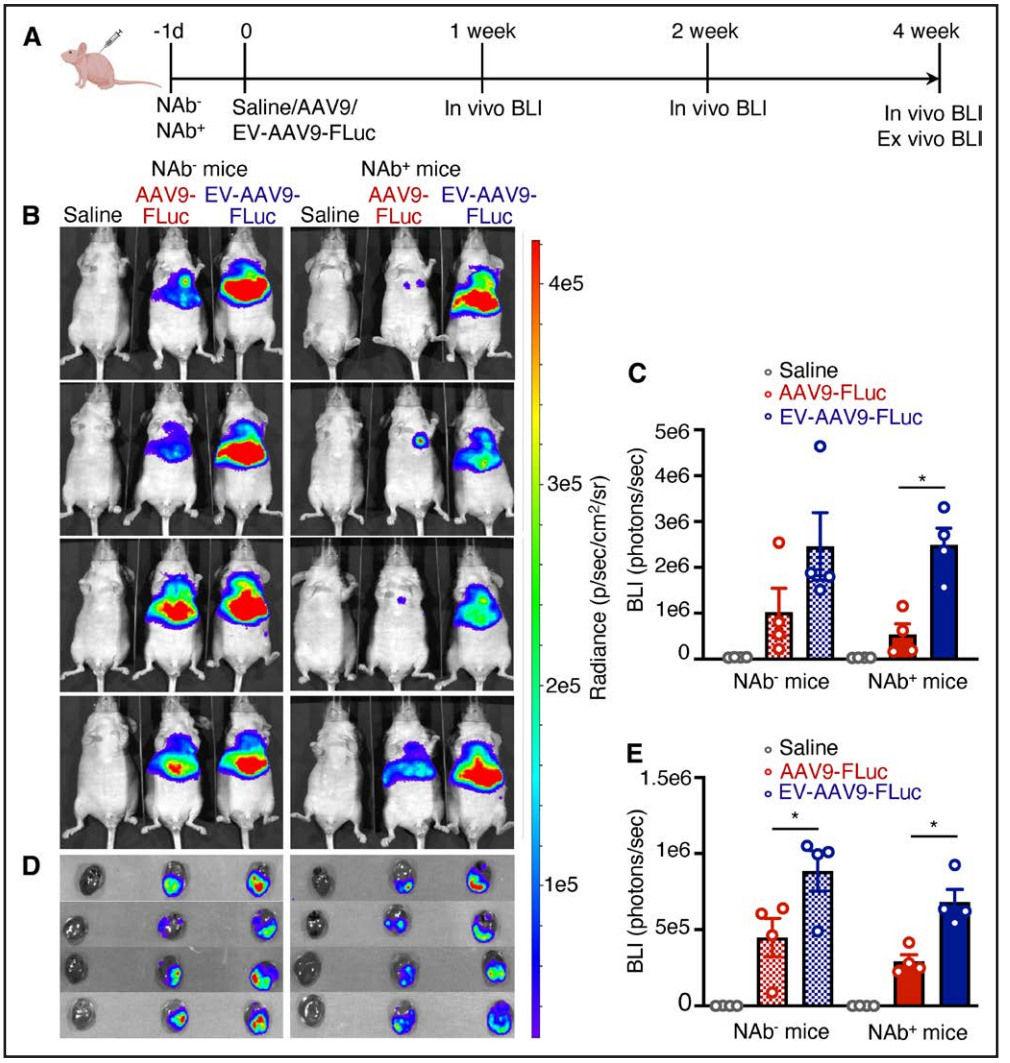

Figure 4. EV-AAVs deliver genes more efficiently than AAVs in the presence of NAb in vivo.
A, Study design**. B**, Bioluminescent images of nude mice at 4 weeks after injection of equal titers (5e10 vector genomes [vg] per mouse) of EV-AAV9–FLuc, AAV9-FLuc, or saline (as an imaging negative control) directly into myocardium. Twenty-four hours before extracellular vesicle–encapsulated adeno-associated vector 9 (EV-AAV9)/AAV9 administration, mice were intravenously injected with saline (neutralizing antibody [NAb] negative) or NAb (NAb⁺; 1 mg NAb per mouse). **C**, Bioluminescent signal quantification of EV-AAV–FLuc, AAV-FLuc, and saline in the heart and liver regions of NAb⁻ and NAb⁺ mice (n=4). **D**, Ex vivo imaging of hearts from NAb⁻ and NAb⁺ mice injected with EV-AAV9–FLuc, AAV9-FLuc, and saline. Mice were euthanized at 4 weeks after EV-AAV9/AAV9 administration; organs were removed and imaged in the IVIS system. **E**, Bioluminescent signal quantitation for EV-AAV, AAV, and saline in ex vivo hearts from NAb⁻ and NAb⁺ mice (n=4). Values in **C** and **E** were analyzed with 2-way ANOVA, and pairwise comparisons were analyzed with the Bonferroni multiple-comparison test. Saline groups were used to assess background (negative controls) and are excluded from analysis. Data are presented as mean±SEM. *$P<0.05$.

those that received conventional free AAV9-SERCA2a or saline (52.2% in EV-AAV9 versus 41.2% in AAV9 and 27.0% in saline control; Figure 5B). In NAb⁺ mice, EF, FS, and cardiac wall motion in the free AAV9–administrated mice were significantly lower than in NAb⁻ mice due to the neutralizing activity of anti-AAV antibodies (Figure 5B through 5D). However, SERCA2a delivery with EV-AAV9 outperformed the free AAV9 group in the presence of NAb, significantly enhancing cardiac function, as demonstrated by elevated EF and FS values (EF, 55.1% versus 27.3%; FS, 32.3% versus 18%; Figure 5B through 5D). We obtained similar EF and FS results at 2 and 4 weeks after surgery (Figure 5E and 5F; Figure S13A through S13D). Furthermore, expression of SERCA2a and a related calcium ion regulator, Ryr2 mRNAs, quantified from left ventricular tissue, was significantly upregulated in the EV-AAV group compared with the AAV group in the presence of NAb at 6 weeks after surgery (Figure S13E and S13F).

Overall, our in vivo functional data demonstrate that EV-AAV9–SERCA2a significantly improved cardiac function compared with AAV9-SERCA2a in the presence of NAb, thereby indicating that EV-AAV vectors can increase the efficacy of AAV-mediated gene therapy in the heart and may potentially be used in humans with preexisting antibodies to AAV.

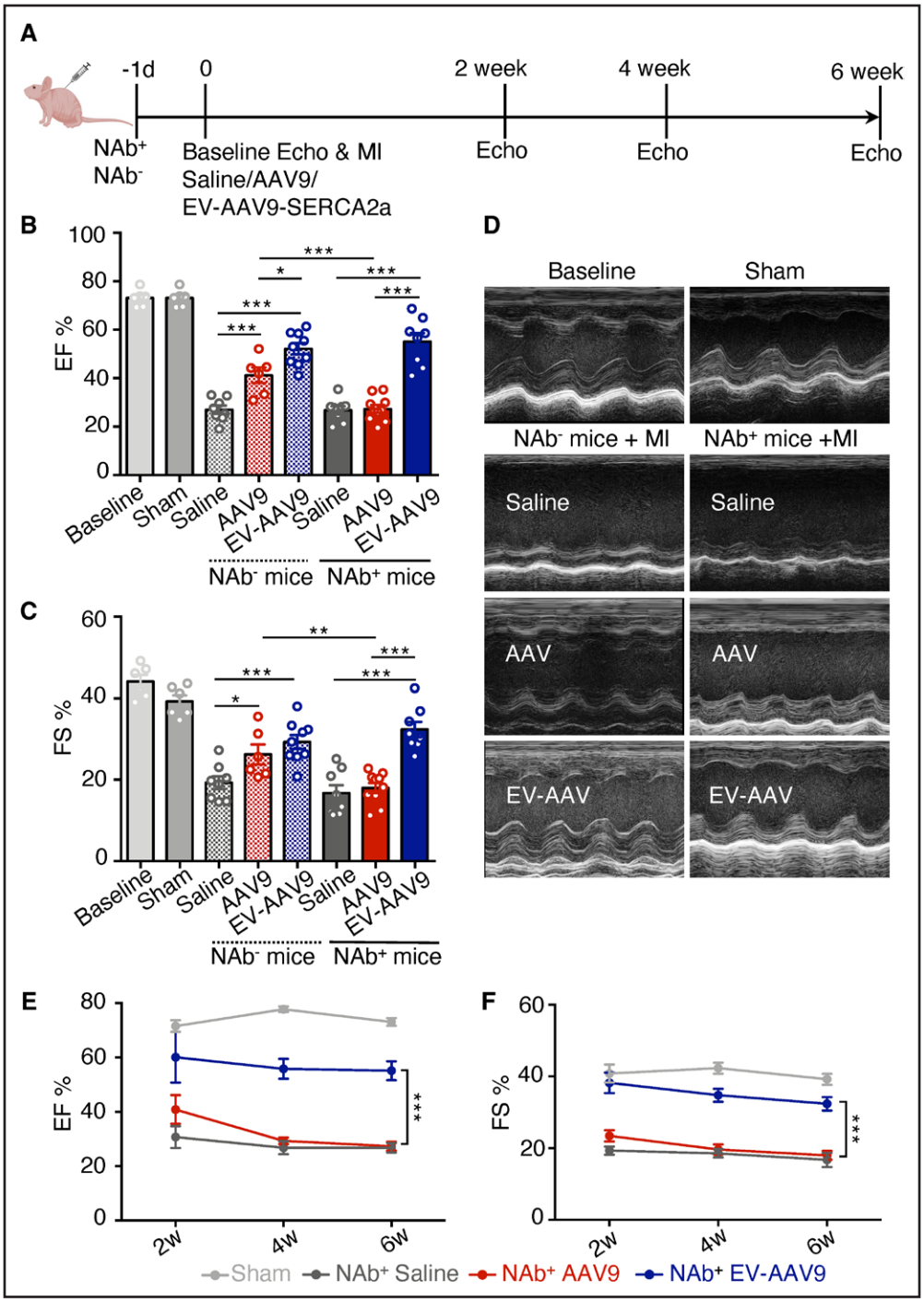

Figure 5. EV-AAV–mediated SERCA2a gene delivery significantly improves cardiac function in the presence of NAb in a preclinical mouse model of MI.

A, Study design. **B**, Echocardiographic assessments of left ventricular function showing ejection fraction (EF; %). **C**, Fractional shortening (FS; %) at 6 weeks after myocardial infarction (MI) in neutralizing antibody (NAb)–negative and NAb$^+$ mice (1 mg NAb per mouse) injected with equal titers (1e11 vector genomes [vg] per mouse) of EV-AAV9–sarcoplasmic reticulum calcium ATPase 2a (SERCA2a), AAV9-SERCA2a, or saline (n=6–10). Data were analyzed with 2-way ANOVA, and pairwise comparisons were analyzed with the Bonferroni multiple-comparison test. Baseline and sham groups were negative controls and were excluded from the statistical comparison. **D**, Representative M-mode echocardiograms showing anterior and posterior left ventricular wall motion at 6 weeks after MI in NAb$^-$ and NAb$^+$ mice. Trend lines for EF (**E**) and FS (**F**) from 2 weeks to 6 weeks after MI. Data were analyzed with 2-way repeated-measures ANOVA followed by the Bonferroni multiple-comparison test for NAb$^+$EV-AAV–SERCA2a group compared with NAb$^+$AAV9–SERCA2a group. Data are presented as mean±SEM. $^*P<0.05$; $^{**}P<0.01$; $^{***}P<0.001$.

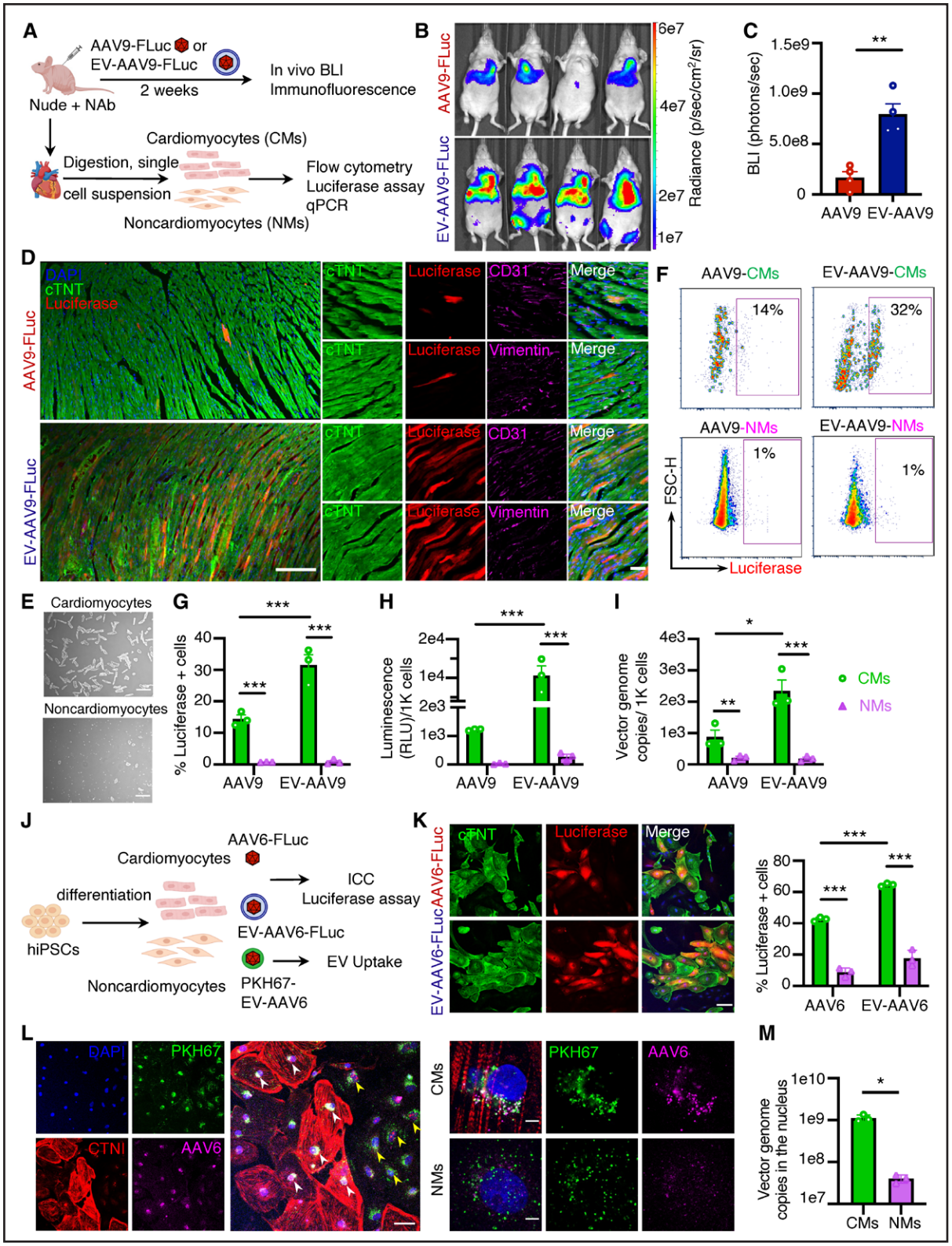

Figure 6. EV-AAVs exhibit cardiotropism.

A, Study design to examine cardiotropism of extracellular vesicle–encapsulated adeno-associated virus 9 (EV-AAV9) in vivo. **B**, In vivo bioluminescent images of nude mice at 2 weeks after intramyocardial injection (1e12 vector genomes [vg] per mouse) of EV-AAV9–FLuc or AAV9-FLuc. Twenty-four hours before EV-AAV9/AAV9 administration, each mouse was intravenously injected with 5 mg of neutralizing antibody (NAb). **C**, Bioluminescent signal quantification of EV-AAV–FLuc or AAV-FLuc in the heart regions (n=4). Data were analyzed with the 2-tailed Student *t* test. **D**, Immunofluorescence images for cTNT, luciferase, CD31, and Vimentin in the left ventricles of hearts from the nude mice at 2 weeks after intramyocardial injection of EV-AAV9–FLuc or AAV9-FLuc. DAPI is shown in blue; cTNT, green; luciferase, red; (*Continued*)

Figure 6 Continued. and CD31/Vimentin, magenta. Scale bar (**left**)=200 μm; **right**=50 μm. **E**, Representative bright-field images of cardiomyocytes (CMs) and noncardiomyocytes (NMs). A Langendorff perfusion method was used to isolate CMs and NMs from mice heart left ventricles. Scale bar=50 μm. **F**, Flow cytometry images and quantification (**G**) of luciferase$^+$ CMs and NMs from the left ventricles injected with EV-AAV9–FLuc or AAV9-FLuc (n=3). **H**, Luciferase activity of CMs and NMs from the left ventricles injected with EV-AAV9–FLuc or AAV9-FLuc (n=3). Values are normalized to 1000 cells. **I**, The vg copies in CMs and NMs from the left ventricle injected with EV-AAV9–FLuc or AAV9-FLuc (n=3). Values are normalized to 1000 cells. **J**, Study design to examine cardiotropism of EV-AAV6 in human induced pluripotent stem cell (hiPSC)–derived CMs and NMs. **K**, Representative immunocytochemistry (ICC) images and quantification for luciferase expression on hiPSC-cTNT$^+$-CMs and cTNT$^-$-NMs transduced with AAV6-FLuc or EV-AAV6–FLuc after 48 hours (multiplicity of infection [MOI], 2e5 vg per cell). DAPI is shown in blue; cTNT, green; and luciferase, red. Scale bar=100 μm. Values in **G** through **I** and **K** were analyzed with 2-way ANOVA, and pairwise comparisons were analyzed with the Bonferroni multiple-comparison test. **L**, Representative ICC images for PKH67, AAV6 and cTNI of cTNI$^+$ hiPSC-CMs, and cTNI$^-$ hiPSC-NMs at 10 hours after incubation with PKH67-labeled EV-AAV6 (MOI; 1e6 vg per cell). DAPI is shown in blue; PKH67, green; cTNI, red; and AAV6, magenta. Scale bar (**left**)=50 μm; **right**=5 μm. **M**, The vg copies in isolated nuclei of hiPSC-CMs and NMs at 24 hours after incubation with EV-AAV6 (MOI; 1e5 vg per cell; n=3). Data were analyzed with the Welch *t* test. **P*<0.05. Data are presented as mean±SEM. ***P*<0.01; ****P*<0.001.

EV-AAVs Exhibit Cardiotropism

Off-target transgene expression in liver remains a major challenge for AAV-mediated gene delivery. BLI images from our in vivo experiments showed both cardiac and liver delivery by EV-AAVs. To compare the gene delivery between the liver and the heart, we quantified both vector genome copy number and transgene expression from the heart and liver cells of the mice injected intramyocardially with AAV9-FLuc or EV-AAV9–FLuc (Figure S14). The vector genome copy number was significantly higher, but luciferase transgene expression was significantly lower in cells isolated from liver compared with both CMs and noncardiomyocytes (NMs) from the heart (Figure S14). This suggests a lack of correlation between vector genome DNA and transgene expression, an observation that has been reported previously.[63]

Our data also showed that EV-AAV–mediated delivery induced higher transgene expression in CMs compared with NMs or liver cells, suggesting a cardiotropic expression. We further investigated the cardiotropic mechanisms of EV-AAV9 in vivo by studying their uptake into cardiac cells by intramyocardially injecting PKH67-labeled EV-AAV9s into nude mice. Flow cytometry data from single-cell suspensions revealed that both CMs and NMs internalized PKH67-EV-AAVs at comparable levels at both 1 and 24 hours (Figure S15). To identify the cell type expressing the transgene, we injected either EV-AAV9–FLuc or AAV9-FLuc intramyocardially, with (Figure 6A) and without (Figure S16A) NAb, and analyzed transgene expression and vector copies in the heart after 2 weeks. In line with our previous data (Figure 4), BLI images showed higher luciferase expression in the hearts delivered by EV-AAVs compared with free AAVs (Figure 6B and 6C; Figure S16B and S16C). Immunofluorescence imaging of the left ventricle revealed that the luciferase-positive cells were predominantly cTNT (cardiac troponin T)$^+$ rod-shaped CMs (Figure 6D; Figure S16D), whereas luciferase-negative cells were largely the NMs, including the CD31$^+$ endothelial cells or Vimentin$^+$ cardiac fibroblasts (Figure 6D). We quantified luciferase expression in the CMs and NMs from the left ventricles (Figure 6A and 6E) using flow cytometry analysis for luciferase$^+$ cells, luciferase expression assay, and vector genome assessment by qPCR. Our data suggest that luciferase expression in CMs was significantly higher than in NMs from both EV-AAV9– and AAV9–injected left ventricles (Figure 6G–6I; Figure S17), implying cardiotropic delivery for both. EV-AAV9 delivered significantly higher luciferase to the CMs compared with AAV9, confirming its superior cardiotropism (Figure 6G–6I; Figures S14 and S17).

To investigate whether EV-AAVs also exhibit cardiotropism in human CMs in vitro, we characterized the transgene expression and uptake of AAV6 and EV-AAV6 in hiPSC-CMs and hiPSC-NMs (Figure 6J). hiPSC-derived cells were treated with an equal titer of EV-AAV6–FLuc or AAV6-FLuc and immunostained to quantify luciferase$^+$ cells. Similar to the cardiotropic expression in mice left ventricles, luciferase was expressed primarily in cTNT$^+$ CMs in both AAV6- and EV-AAV6–infected hiPSC-derived cells (Figure 6K). In particular, EV-AAV6 transduced the hiPSC-CMs with significantly greater efficiency compared with AAV6 (Figure 6K). In the same line, fluorescence-activated cell–sorted SIRPA (signal regulatory protein alpha)$^+$CD90$^-$ hiPSC-CMs had significantly higher luciferase expression compared with SIRPA$^-$CD90$^+$ NMs transduced with an equal titer of EV-AAV6–FLuc or AAV6-FLuc (Figure S18), confirming cardiotropic delivery of EV-AAVs to hiPSC-CMs.

In line with the in vivo uptake of EV-AAVs, uptake of PKH67-labeled EV-AAV6 in hiPSC-derived cells showed internalization by both cTNI (cardiac troponin I)$^+$CMs and cTNI$^-$NMs (Figure 6L; Figure S19). However, in hiPSC-CMs, the uptaken EV-AAVs were detected around the perinuclear region (stronger green and magenta staining at 10 hours), whereas in hiPSC-NMs, they appeared diffused in the cytoplasm, suggesting a distinct intracellular trafficking between CMs and NMs (Figure 6L, right). Nuclear entry of AAV is a critical step for successful transgene expression.[64] To compare the nuclear entry and genome release of AAV particles between hiPSC-CMs and NMs, we infected each with equal amounts of EV-AAV6 and quantified the vector genomes by qPCR in the extracted nuclei after 24 hours. EV-AAVs delivered a significantly higher quantity of vector genome into the nucleus of hiPSC-CMs compared with NMs (Figure 6M). This suggests a distinction in the postlysosomal nuclear entry between CMs and NMs, which may play a role in the cardiotropic mechanism of EV-AAV. In

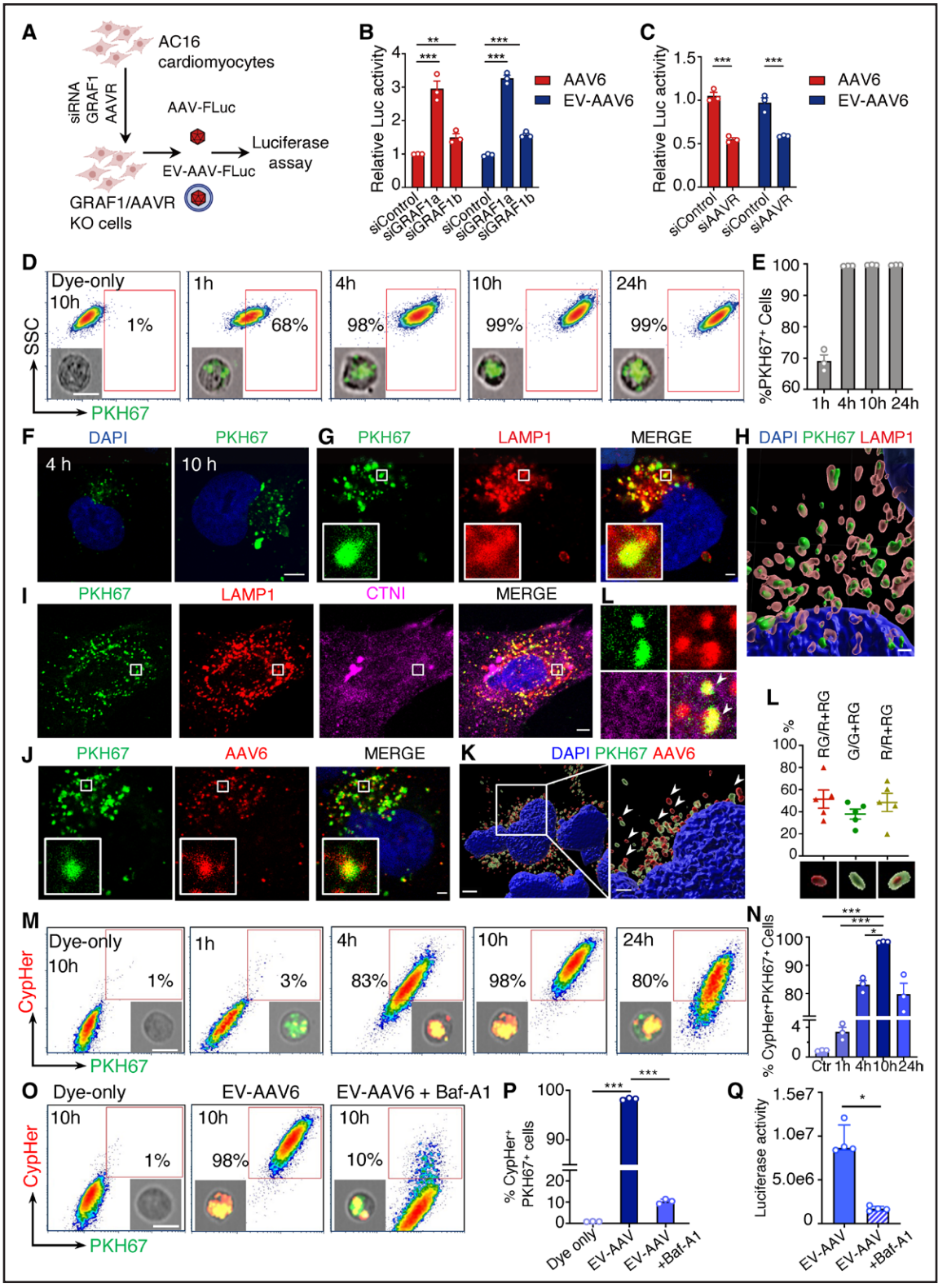

Figure 7. EV-AAV uptake involves trafficking through endocytic/acidic compartments.
A, Study design to examine involvement of endocytic pathway and adeno-associated virus (AAV) receptors (AAVRs). **B**, Relative transduction efficiency of EV-AAV6–FLuc and AAV6-FLuc in hAC16 cardiomyocytes (CMs) after GRAF1 or AAVR knockdown by siRNA (**C**). Relative luciferase activities are normalized to each siRNA control. Data were analyzed with 2-way ANOVA followed by Dunnett multiple-comparison test (n=3). **D**, Flow cytometry analysis showing PKH67-labeled extracellular vesicle–encapsulated AAV6 (EV-AAV6) uptake in hAC16-CMs at different time points. Scale bar=20 μm. **E**, Quantification of PKH67⁺ hAC16-CMs at 1, 4, 10, and 24 hours (n=3). **F**, Confocal microscopy analysis showing the internalization of PKH67-labeled EV-AAV6 in hAC16-CMs at 4 and 10 hours. Scale bar=5 μm. **G**, (*Continued*)

Figure 7 Continued. Immunostaining for LAMP1 on hAC16-CMs at 10 hours after incubation with PKH67-labeled EV-AAV6 (blue, DAPI; green, PKH67-labeled EV-AAV; red, LAMP1; yellow, colocalization of PKH67 and LAMP1). Scale bar=2 μm. **H**, Three-dimensional visualization showing the colocalization of PKH67-labeled EV-AAV6 and LAMP1+ subcompartments performed with Imaris 9.8. Scale bar, 2 μm. **I**, Immunostaining for LAMP1 on hiPSC-CMs at 10 hours after incubation with PKH67-labeled EV-AAV6. DAPI is shown in blue; PKH67-labeled EV-AAV, green; LAMP1, red; and cTNI, magenta. White arrows show colocalization of PKH67 and LAMP1. Scale bar=5 μm. **J**, Immunostaining for intact AAV6 particles on hAC16 cells at 10 hours after incubation with PKH67-labeled EV-AAV. Scale bar=2 μm. **K**, Three-dimensional visualization showing the colocalization or delocalization of PKH67-labeled EV-AAV6 and AAV6 performed with an Imaris 9.8. White arrows point to released free AAVs labeled in red. Scale bar (**left**)=5 μm; **right**=2 μm. **L**, Quantification of the PKH67 and AAV colocalization in **K**: green (G), PKH67; red (R), AAV6; red and green (RG; n=5). **M**, Flow cytometry analysis and quantification (**N**) showing PKH67 and CypHer-labeled EV-AAV6 uptake in hAC16-CMs at different time points (n=3). Scale bar=20 μm. Data were analyzed with the Welch 1-way ANOVA followed by Dunnett-T3 multiple-comparison test. **O**, Flow cytometry analysis and quantification (**P**) showing PKH67 and CypHer-labeled EV-AAV6 uptake in hAC16-CMs at 10 hours after treatment with bafilomycin A1 (Baf-1A; n=3). Scale bar=20 μm. Data were analyzed with 1-way ANOVA followed by the Tukey multiple-comparison test. **Q**, Luciferase activity of hAC16-CMs transduced with EV-AAV6 after 48 hours. hAC16-CMs were treated with dimethyl sulfoxide (DMSO) or Baf-1A for 2 hours before transduction with EV-AAV6 (n=4). Data are presented as median±interquartile range and were analyzed with the Mann-Whitney *U* test. Values in **B**, **C**, **E**, **L**, **N**, and **P** are presented as mean±SEM. **P*<0.05; ***P*<0.01; ****P*<0.001.

summary, these data demonstrate superior cardiotropism of EV-AAV9 in vivo and EV-AAV6 in vitro.

EV-AAV Transduction Is Dependent on AAV Receptor

To gain mechanistic insights into EV-AAV–mediated cardiac gene delivery, we studied its uptake and transduction in CMs. AAV transduction is a multistep process that includes several endocytic internalization routes, sorting and acidification in the cytoplasm, nuclear entry, and transgene expression.[64–66] In contrast, the mechanisms of EV-AAV uptake, intracellular trafficking, and AAV release from EV-AAVs have not been studied yet. Uptake of certain AAV serotypes (eg, AAV2) have been shown to be mediated by the well-characterized clathrin-independent carriers (CLICs) in glycosylphosphatidylinositol-anchored protein-enriched endosomal compartments (GEECs), CLIC/GEEC.[65,67] Knocking down RhoGTPase-activating protein GRAF1, a critical regulator of GLIC/GEEC endocytosis, in hAC16-CMs (Figure S20A and S20B) did not inhibit AAV6/9 or EV-AAV6/9 transduction (Figure 7A and 7B; Figure S20C and S20D); on the contrary, it significantly increased it. This suggests that the GRAF1-mediated CLIC/GEEC pathway did not facilitate the internalization of EV-AAV6/9 and AAV6/9 but negatively regulated their uptake and expression in hAC16-CMs. Next, we tested whether another essential AAV receptor (AAVR; a recycling receptor trafficking AAVs to the trans-Golgi network [TGN]),[68,69] shown to facilitate AAV6/9 infection, is required for EV-AAV transduction. Knocking down AAVR (Figure S20E and S20F) in hAC16-CMs resulted in significant inhibition in the transduction efficiency of both AAV6/9 and EV-AAV6/9 (Figure 7A and 7C; Figure S20G and S20H), suggesting that infection of both AAV6/9 and EV-AAV6/9 was dependent on AAVR.

EV-AAV Uptake Involves Trafficking Through Acidic Compartments

To investigate the mechanisms of EV-AAV intracellular trafficking, we examined the uptake of PKH67-labeled EV-AAV6s to different cellular compartments of hAC16-CMs in vitro. Flow cytometry analysis of PKH67-EV-AAV6 at different time points showed partial internalization of EV-AAV6 by the treated cells at 1 hour and almost complete internalization at 4 to 24 hours (Figure 7D and 7E; Figure S21A). High-resolution confocal microscopy analysis detected PKH67-EV-AAV6 with markers of early endosomes (Rab5; modest presence at 4 hours), late endosomes (Rab7; at 10 hours), and lysosomes (LAMP1; at 10 hours), suggesting that these cytoplasmic compartments had internalized EV-AAV (Figure 7F through 7H; Figure S21B and S21C). Consistent with hAC16-CM uptake, hiPSC-CMs incubated with PKH67-EV-AA6 showed EV-AAVs colocalized with LAMP1+ lysosomes at 10 hours (Figure 7I).

To address whether EV-AAVs were intact (ie, the EVs still enveloped the AAVs), we co-stained the PKH67-EV-AAV6s with anti-AAV6 antibody (which detects intact AAV6 particles) in hAC16-CMs and hiPSC-CMs. We observed partial colocalization of PKH67-EV-AAV6 with AAV6 in punctate structures within the cytoplasm at 4 to 10 hours, the point at which the PKH67-EV-AAVs colocalized with late endosome/lysosome (Figure 7J; Figure S22A). These data suggest that at 4 to 10 hours of uptake, EV-AAVs are in the process of releasing AAVs in both hAC16-CMs and hiPSC-CMs. Intracellular trafficking of AAVs may follow a different time line; they are found in the nucleus in hiPSC-CMs at 10 hours (Figure S22B). Our 3-dimensional model reconstruction and colocalization analysis of the same images, obtained at 10 hours, confirmed that ≈50% of the vesicles were still intact (stained with both PKH67 and AAV6), and ≈50% were separated (stained with either PKH67 or AAV6; Figure 7K and 7L). These results indicate that EV-AAVs might be internalized by late endosomes/lysosomes, possibly undergo acidification, and release AAVs before they enter the nucleus.

AAV acidification is an important step in their delivery to the nucleus. To investigate whether EV-AAVs were taken up by acidic subcompartments, we labeled EV-AAV6s with both PHK67 dye, to track EV-AAV trafficking in the cytoplasm, and CypHer dye (a pH-sensitive

dye that is fluorescent at an acidic pH), to track EV-AAV uptake into acidic cytoplasmic vesicles, and incubated with hAC16-CMs for 1, 4, 10, and 24 hours before flow cytometry and imaging analysis. We observed that the percentage of PKH67$^+$CypHer$^+$ cells maximized at 10 hours (98.28±0.12%), demonstrating that EV-AAVs sorted into subcellular compartments with acidic pH (Figure 7M and 7N; Figure S23). This finding is in line with our previous observation of EV-AAV uptake to LAMP1$^+$ compartments at 10 hours. To confirm this, we pretreated hAC16-CMs with bafilomycin A1, a V-ATPases inhibitor that blocks the acidification of endosomal/lysosomal compartments,[70] followed by incubation with PKH67-CypHer-EV-AAV6s. We found that the majority of the PKH67-EV-AAV6s were still internalized (≈98% PKH67$^+$ cells at 10 hours) but not in the acidic compartments (≈10% CypHer$^+$ cells at 10 hours; Figure 7O and 7P; Figure S23). Lack of acidification of endosomal/lysosomal compartments (bafilomycin A1–pretreated cells) significantly decreased the transduction efficiency of EV-AAV (Figure 7Q). Together, these data suggest that EV-AAVs are internalized to the acidic compartments of endosomes/lysosomes, in which the EV-AAVs might be released, and AAVs may be acidified for further transport into the nucleus.

DISCUSSION

In this study, we demonstrated the functional benefits and mechanisms of EV-AAVs, a superior vector that offers NAb resistance and delivers therapeutic genes to ischemic hearts. We optimized an EV-AAV purification strategy, comprehensively characterized EV-AAVs, used 5 different in vitro and in vivo model systems to demonstrate significantly higher potency and therapeutic efficacy of EV-AAVs, and compared that with free AAVs. We also reported a mechanism of uptake and cardiotropism of EV-AAV vectors.

AAV-mediated transgene expression in the myocardium has low efficiency (0.5%–2.6%).[71] Enhancing the transduction efficiency of viral genome delivered to the heart is significant for developing AAV-based cardiac gene therapy. Our study has uncovered that EV-AAVs consistently deliver more genes to CMs compared with free AAVs both in vitro and in vivo, even in the absence of NAbs (although in some cases, it was not statistically significant; Figures 3F and 4C; Figure S16C). Previous studies have shown that FBS can inhibit AAV6 transduction in cell culture.[72] In our experiments, the presence of 10% FBS in cell culture of hAC16-CMs significantly inhibited AAV6 transduction but not EV-AAV6 transduction (Figure S24). Preexisting antibodies against the cardiotropic AAV serotypes AAV1, AAV6, and AAV9 and against AAV2 in mice from commercial vendors,[19] as well as murine[73] and bovine AAVs,[74] have also been reported previously. It is possible that the presence of preexisting NAbs in mice and FBS in our experiments neutralizes free AAVs to a certain extent and benefits EV-AAVs. EV-AAVs demonstrate significantly higher transduction efficiency compared with free AAVs when infected to hiPSC-CMs, which were cultured without FBS. Besides, in both hiPSC-derived cells and mice, EV-AAVs expressed more transgenes in CMs compared with NMs, even with equivalent cellular uptake. Higher transgene expression of EV-AAVs in hiPSC-CMs was consistent with significantly higher nuclear entry of vector genome compared with NMs (Figure 6M). The cardiotropic expression of EV-AAVs could be due to one or more of the following: (1) Because NMs, including fibroblasts and endothelial cells, proliferate at higher rates than CMs,[75] the delivered gene can be lost during proliferation (the recombinant AAV genome rarely undergoes site-specific integration in host DNA and persists largely as an episome).[12–14,18] (2) Uptaken EV-AAVs have differential cytoplasmic processing[76] and endosomal/lysosomal degradation and release[77] between CMs and NMs (Figure 6L and 6M). (3) Intracellular trafficking, conformational changes of the AAV capsid in the cytoplasm, interaction between capsid and nuclear pore complexes, and postlysosomal nuclear entry of AAVs[64] and EV-AAVs could be different in different cell types. Deciphering the mechanism of EV-AAV uptake and transgene expression in CMs will provide new insights into augmenting AAV transduction therein.

A detailed picture of AAV cellular entry and uptake mechanisms is now emerging.[65,78] Different AAV serotypes may have similar or distinct uptake pathways, which may also be recipient cell–type dependent. AAV capsids bind to receptors on the host cell surface, are internalized through multiple endocytic routes, and undergo conformational changes through endosome/Golgi retrograde transport or late endosome/lysosome pathway, followed by cytoplasmic escape and nuclear import.[64,65] The EV-AAV uptake mechanisms have not been studied yet. Our study revealed that infection of both AAV6/9 and EV-AAV6/9 was dependent on AAVR but not on GRAF1-dependent CLIC/GEEC. These data suggest that AAVR could be a common receptor for AAVs and EV-AAVs and may have a broader function than previously known.

For successful transduction, AAV must escape from the subcellular compartments to the acidic pH in the endosome and lysosome before entering the nucleus. Like AAVs, EVs undergo endocytosis and release cargos in acidic compartments. Endosomal acidification has been shown to facilitate EV cargo function.[77] In line with other reports on EV uptake,[77,79] we showed here that EV-AAVs colocalize with bafilomycin-sensitive low-pH compartments in late endosomes and lysosomes, from which they release AAVs (Figures 7 and 8). This work reveals 2 important steps in the expression of genes carried by EV-AAVs: delivering AAV cargo, and preparing AAV for its nuclear translocation. It is worth noting that

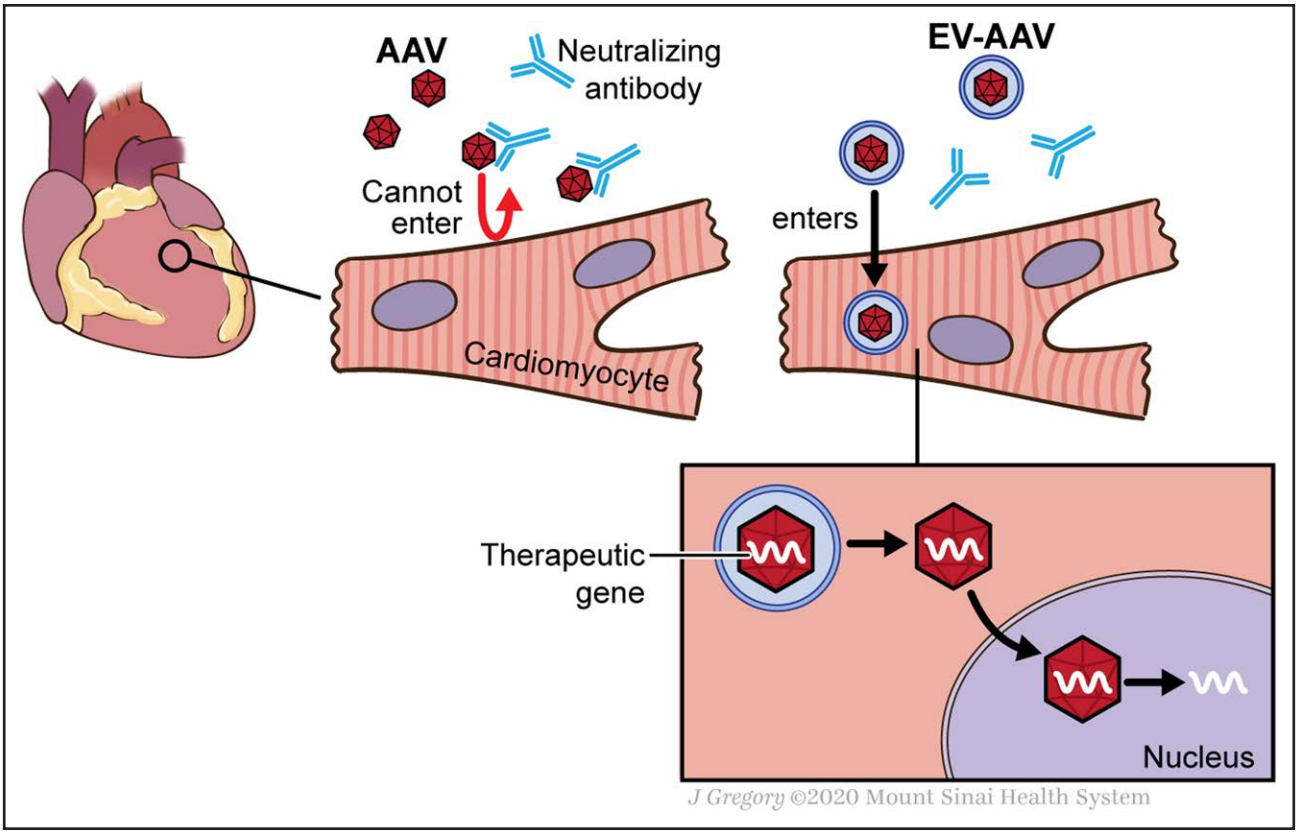

Figure 8. Schematic of EV-AAV uptake in cardiomyocytes.
Free adeno-associated viruses (AAVs) bind with neutralizing antibodies that block AAV delivery into cells. Extracellular vesicle–encapsulated AAVs (EV-AAVs) protect the AAVs from this neutralizing effect to improve gene delivery to cardiomyocytes. In the cytoplasm, EV-AAVs are taken up into acidic subcellular compartments such as late endosomes and lysosomes, which may release the AAVs from EV-AAVs, thereby enabling nuclear entry and gene expression. Reprinted with permission from Mount Sinai Health System.

AAV particle degradation before nuclear entry leads to low transduction. Our data show that EV-AAVs have significantly higher transduction efficiency than free AAVs even without NAbs, thereby indicating that EV-AAVs might protect AAV from degradation before it enters the nucleus, as observed in EV-AAV membrane separation from the AAV cargo that it delivers. An endosomal pathway to the TGN exists for AAV transduction[80]; however, whether EVs undergo retrograde trafficking to the TGN is poorly understood.[81] AAVR may play a role in cell surface attachment of AAVs, trafficking AAV particles to TGN, or the escape of AAVs out of TGN.[68,69,82] The inhibition of EV-AAV transduction in AAVR-knockdown cells (Figure S20E through S20H) suggests that either the AAVR-mediated intracellular trafficking of AAVs (which are released from EV-AAVs) to TGN is impaired or AAVR directly regulates EV-AAV uptake and intracellular processing independently of its regulation of free AAV capsid trafficking, thereby affecting the internalization and transduction of EV-AAVs. Uncovering the underlying mechanism for EV-AAV trafficking requires deeper investigation. Distinct mechanisms between AAVs and EV-AAVs could have important therapeutic implications and need further investigation. Taken together, our findings on EV-AAV trafficking provide novel insights into EV-AAV content delivery to and function in recipient CMs.

Our study demonstrates the NAb evasion and preclinical benefits of EV-AAV vectors for therapeutic gene delivery to the heart after myocardial ischemia and addresses knowledge gaps in their biology and cellular trafficking mechanisms. The benefits of EV-AAV–mediated gene delivery are multifold. First, because their robust exosomal membrane can protect AAVs from being accessed by NAbs, EV-AAVs have higher resistance to NAb,[34] and EV-AAV–mediated delivery will facilitate repeated dosing in patients. Moreover, because exosomes are structurally sturdier than other EVs,[42,83] they may be good therapeutic vehicles. Second, EVs and EV-AAVs can be rapidly taken up by target cells[84,85] such as CMs and thus can efficiently deliver genes to the dynamic cardiac environment heart. Third, EVs outperform synthetic nanovesicles in stability, uptake, and gene delivery efficiency.[86]

By deciphering the molecular uptake mechanisms of EV-AAV, compartmentalized cellular signaling, and enhanced expression in CMs, our findings may provide important insights into AAV-mediated gene delivery and

cardioprotection. Although our investigation established the proof of concept for successfully using EV-AAVs to deliver genes to the heart in the presence of NAbs, ultracentrifugation-based methods are time-consuming and inefficient and result in low yield, making them unsuitable for the high-throughput production needed for clinical use. Therefore, newer methods need to be tested to efficiently separate AAV contaminants from EV-AAVs to accurately evaluate their purity for future preclinical and clinical applications.

Our results offer a thorough overview of the gene delivery potential of EV-AAVs and their suitability as a vector for AAV delivery, in the presence of NAbs, to the myocardium. EVs, in general, do not exhibit cell and tissue tropism yet show different rates of uptake by different cells.[81] Therefore, to improve their expression in the heart, we delivered EV-AAVs intramyocardially. Local delivery methods were preferred routes as well in earlier studies with EV-AAV–mediated delivery to other organs such as the retina and brain.[28,29,33,34,87] Nonetheless, genes delivered to the heart through EV-AAVs, similar to those delivered through AAVs, are associated with off-target expression such as in the liver, even with local intramyocardial delivery. Intramyocardial delivery of EV-AAVs is an invasive procedure and could be a limitation to the EV-AAV–mediated gene delivery. Thus, a CM-targeting strategy for EV-AAVs using engineered AAVs[88] with improved potency for cardiac or muscle delivery[63] may confine gene expression to the heart and may hold a key to their successful clinical translation. All previous studies, including ours, observed good cell tolerance of EV-AAVs with no side effects. Nevertheless, future investigations into their long-term efficiency, safety, dosing, and biodistribution are necessary. There are a few functional studies on EV-mediated gene delivery to the brain, retina, and cancerous cells, but the uptake and delivery mechanisms of EV-AAVs had not been investigated before our study. Advancing EV-AAV therapies to the clinic will require quantitative, mechanism-driven analyses of EV-mediated delivery.

Collectively, our work here confirms that EV-AAVs are fully infectious, resist antibody-mediated neutralization, and can efficiently transduce the myocardium. Our investigation provides advanced strategies to improve gene therapy by circumventing NAb neutralization, which has been a roadblock to previous efforts in the field. These findings open a new avenue for clinically translating AAV-based cardiac gene therapies to treat a broader population of patients with heart failure. In summary, our study will positively affect future preclinical studies and clinical trials in gene therapy and has the potential to advance current AAV-based therapeutic applications for treating cardiovascular diseases.

ARTICLE INFORMATION

Received December 23, 2022; accepted May 16, 2023.

Affiliations

Cardiovascular Research Institute (X.L., S.L.S., M.A., E.C., D.C., E.L.-G., S.Y., N.A., D.J., S.L., A.P., N.R., S.Z., L.Z., S.S.), Department of Oncological Sciences (E.G.-K.), Department of Pathology and Laboratory Medicine (N. Dogra), Icahn Genomics Institute (N.Dogra), Department of Cell, Developmental and Regenerative Biology (N. Dubois), and Mindich Child Health and Development Institute (N. Dubois), Icahn School of Medicine at Mount Sinai, New York, NY. Center for Biological Science and Technology, Advanced Institute of Natural Sciences, Beijing Normal University, Zhuhai, China (Y.L.). Benthos Prime Central, Houston, TX (P.M.). Spark Therapeutics, Philadelphia, PA (E.K.). Department of Molecular and Life Science, College of Science and Convergence Technology, Hanyang University-ERICA, Ansan, South Korea (D.J.). NanoView Biosciences, Boston, MA (G.D.). Gene and Cell Therapy Institute, Massachusetts General Brigham, Boston (R.J.H.).

Acknowledgments

The authors acknowledge the contribution from Drs Lauren Wills, Thomas Weber, and Brent A. French for providing some of the gene vectors used in this study; William Jenssen for acquiring EM pictures; Lifan Liang for in vitro luciferase assay; and Jill K. Gregory for assistance with graphic illustrations. This work was supported in part through the computational resources and staff expertise provided by Scientific Computing at the Icahn School of Medicine at Mount Sinai.

Sources of Funding

This work was supported by grants from the National Institutes of Health (HL140469, HL124187, HL148786, and DK125856 to Dr Sahoo); New York State Stem Cell Science C32562GG to Dr Sahoo; American Heart Association (17GRNT33460554 to Dr Sahoo); American Heart Association postdoctoral grants (17POST33670354 to Dr Mathiyalagan and 17POST33410648 to Dr Liang); and Hiroshima University funding support to Dr La Salvia.

Disclosures

None.

Supplemental Material

Expanded Methods
Figures S1–S24
Table S1 and S2
References 89–107

REFERENCES

1. Ginn SL, Amaya AK, Alexander IE, Edelstein M, Abedi MR. Gene therapy clinical trials worldwide to 2017: an update. *J Gene Med*. 2018;20:e3015. doi: 10.1002/jgm.3015
2. US Food and Drug Administration. Approved cellular and gene therapy products. Accessed September 1, 2022. https://fda.gov/vaccines-blood-biologics/cellular-gene-therapy-products/approved-cellular-and-gene-therapy-products
3. MacLaren RE, Groppe M, Barnard AR, Cottriall CL, Tolmachova T, Seymour L, Clark KR, During MJ, Cremers FP, Black GC, et al. Retinal gene therapy in patients with choroideremia: initial findings from a phase 1/2 clinical trial. *Lancet*. 2014;383:1129–1137. doi: 10.1016/S0140-6736(13)62117-0
4. Rangarajan S, Walsh L, Lester W, Perry D, Madan B, Laffan M, Yu H, Vettermann C, Pierce GF, Wong WY, et al. AAV5-factor VIII gene transfer in severe hemophilia A. *N Engl J Med*. 2017;377:2519–2530. doi: 10.1056/NEJMoa1708483
5. Ribeil JA, Hacein-Bey-Abina S, Payen E, Magnani A, Semeraro M, Magrin E, Caccavelli L, Neven B, Bourget P, El Nemer W, et al. Gene therapy in a patient with sickle cell disease. *N Engl J Med*. 2017;376:848–855. doi: 10.1056/NEJMoa1609677
6. Greenberg B, Butler J, Felker GM, Ponikowski P, Voors AA, Desai AS, Barnard D, Bouchard A, Jaski B, Lyon AR, et al. Calcium Upregulation by Percutaneous Administration of Gene Therapy in Patients With Cardiac Disease (CUPID 2): a randomised, multinational, double-blind, placebo-controlled, phase 2b trial. *Lancet*. 2016;387:1178–1186. doi: 10.1016/S0140-6736(16)00082-9
7. Jessup M, Greenberg B, Mancini D, Cappola T, Pauly DF, Jaski B, Yaroshinsky A, Zsebo KM, Dittrich H, Hajjar RJ; Calcium Upregulation by Percutaneous Administration of Gene Therapy in Cardiac Disease (CUPID) Investigators. Calcium Upregulation by Percutaneous Administration of Gene Therapy in Cardiac Disease (CUPID): a phase 2 trial of intracoronary gene therapy of sarcoplasmic reticulum Ca2+-ATPase in patients with advanced heart failure. *Circulation*. 2011;124:304–313. doi: 10.1161/CIRCULATIONAHA.111.022889

8. Hammond HK, Penny WF, Traverse JH, Henry TD, Watkins MW, Yancy CW, Sweis RN, Adler ED, Patel AN, Murray DR, et al. Intracoronary gene transfer of adenylyl cyclase 6 in patients with heart failure: a randomized clinical trial. *JAMA Cardiol*. 2016;1:163–171. doi: 10.1001/jamacardio.2016.0008
9. Kieserman JM, Myers VD, Dubey P, Cheung JY, Feldman AM. Current landscape of heart failure gene therapy. *J Am Heart Assoc*. 2019;8:e012239. doi: 10.1161/JAHA.119.012239
10. Niwano K, Arai M, Koitabashi N, Watanabe A, Ikeda Y, Miyoshi H, Kurabayashi M. Lentiviral vector-mediated SERCA2 gene transfer protects against heart failure and left ventricular remodeling after myocardial infarction in rats. *Mol Ther*. 2008;16:1026–1032. doi: 10.1038/mt.2008.61
11. Merten O-W, Gaillet B. Viral vectors for gene therapy and gene modification approaches. *Biochem Eng J*. 2016;108:98–115. doi: 10.1016/j.bej.2015.09.005
12. Smith RH. Adeno-associated virus integration: virus versus vector. *Gene Ther*. 2008;15:817–822. doi: 10.1038/gt.2008.55
13. Valdmanis PN, Lisowski L, Kay MA. rAAV-mediated tumorigenesis: still unresolved after an AAV assault. *Mol Ther*. 2012;20:2014–2017. doi: 10.1038/mt.2012.220
14. Li H, Malani N, Hamilton SR, Schlachterman A, Bussadori G, Edmonson SE, Shah R, Arruda VR, Mingozzi F, Wright JF, et al. Assessing the potential for AAV vector genotoxicity in a murine model. *Blood*. 2011;117:3311–3319. doi: 10.1182/blood-2010-08-302729
15. Flotte TR, Berns KI. Adeno-associated virus: a ubiquitous commensal of mammals. *Hum Gene Ther*. 2005;16:401–407. doi: 10.1089/hum.2005.16.401
16. Herzog RW, Yang EY, Couto LB, Hagstrom JN, Elwell D, Fields PA, Burton M, Bellinger DA, Read MS, Brinkhous KM, et al. Long-term correction of canine hemophilia B by gene transfer of blood coagulation factor IX mediated by adeno-associated viral vector. *Nat Med*. 1999;5:56–63. doi: 10.1038/4743
17. Wang Z, Zhu T, Qiao C, Zhou L, Wang B, Zhang J, Chen C, Li J, Xiao X. Adeno-associated virus serotype 8 efficiently delivers genes to muscle and heart. *Nat Biotechnol*. 2005;23:321–328. doi: 10.1038/nbt1073
18. Penaud-Budloo M, Le Guiner C, Nowrouzi A, Toromanoff A, Cherel Y, Chenuaud P, Schmidt M, von Kalle C, Rolling F, Moullier P, et al. Adeno-associated virus vector genomes persist as episomal chromatin in primate muscle. *J Virol*. 2008;82:7875–7885. doi: 10.1128/JVI.00649-08
19. Rapti K, Louis-Jeune V, Kohlbrenner E, Ishikawa K, Ladage D, Zolotukhin S, Hajjar RJ, Weber T. Neutralizing antibodies against AAV serotypes 1, 2, 6, and 9 in sera of commonly used animal models. *Mol Ther*. 2012;20:73–83. doi: 10.1038/mt.2011.177
20. Naim C, Yerevanian A, Hajjar RJ. Gene therapy for heart failure: where do we stand?. *Curr Cardiol Rep*. 2013;15:333. doi: 10.1007/s11886-012-0333-3
21. Louis Jeune V, Joergensen JA, Hajjar RJ, Weber T. Pre-existing anti-adeno-associated virus antibodies as a challenge in AAV gene therapy. *Hum Gene Ther Methods*. 2013;24:59–67. doi: 10.1089/hgtb.2012.243
22. Hanna E, Rémuzat C, Auquier P, Toumi M. Gene therapies development: slow progress and promising prospect. *J Mark Access Health Policy*. 2017;5:1265293. doi: 10.1080/20016689.2017.1265293
23. Gwathmey JK, Yerevanian A, Hajjar RJ. Targeting sarcoplasmic reticulum calcium ATPase by gene therapy. *Hum Gene Ther*. 2013;24:937–947. doi: 10.1089/hum.2013.2512
24. Calcedo R, Vandenberghe LH, Gao G, Lin J, Wilson JM. Worldwide epidemiology of neutralizing antibodies to adeno-associated viruses. *J Infect Dis*. 2009;199:381–390. doi: 10.1086/595830
25. Greenberg B, Butler J, Felker GM, Ponikowski P, Voors AA, Pogoda JM, Provost R, Guerrero J, Hajjar RJ, Zsebo KM. Prevalence of AAV1 neutralizing antibodies and consequences for a clinical trial of gene transfer for advanced heart failure. *Gene Ther*. 2016;23:313–319. doi: 10.1038/gt.2015.109
26. Feng Z, Hensley L, McKnight KL, Hu F, Madden V, Ping L, Jeong SH, Walker C, Lanford RE, Lemon SM. A pathogenic picornavirus acquires an envelope by hijacking cellular membranes. *Nature*. 2013;496:367–371. doi: 10.1038/nature12029
27. Gyorgy B, Sage C, Indzhykulian AA, Scheffer DI, Brisson AR, Tan S, Wu X, Volak A, Mu D, Tamvakologos PI, et al. Rescue of hearing by gene delivery to inner-ear hair cells using exosome-associated AAV. *Mol Ther*. 2017;25:379–391. doi: 10.1016/j.ymthe.2016.12.010
28. Hudry E, Martin C, Gandhi S, Gyorgy B, Scheffer DI, Mu D, Merkel SF, Mingozzi F, Fitzpatrick Z, Dimant H, et al. Exosome-associated AAV vector as a robust and convenient neuroscience tool. *Gene Ther*. 2016;23:819. doi: 10.1038/gt.2016.65
29. Maguire CA, Balaj L, Sivaraman S, Crommentuijn MH, Ericsson M, Mincheva-Nilsson L, Baranov V, Gianni D, Tannous BA, Sena-Esteves M, et al. Microvesicle-associated AAV vector as a novel gene delivery system. *Mol Ther*. 2012;20:960–971. doi: 10.1038/mt.2011.303
30. Meliani A, Boisgerault F, Fitzpatrick Z, Marmier S, Leborgne C, Collaud F, Simon Sola M, Charles S, Ronzitti G, Vignaud A, et al. Enhanced liver gene transfer and evasion of preexisting humoral immunity with exosome-enveloped AAV vectors. *Blood Adv*. 2017;1:2019–2031. doi: 10.1182/bloodadvances.2017010181
31. Ramakrishnaiah V, Thumann C, Fofana I, Habersetzer F, Pan Q, de Ruiter PE, Willemsen R, Demmers JA, Stalin Raj V, Jenster G, et al. Exosome-mediated transmission of hepatitis C virus between human hepatoma Huh7.5 cells. *Proc Natl Acad Sci USA*. 2013;110:13109–13113. doi: 10.1073/pnas.1221899110
32. Schiller LT, Lemus-Diaz N, Rinaldi Ferreira R, Boker KO, Gruber J. Enhanced production of exosome-associated AAV by overexpression of the tetraspanin CD9. *Mol Ther Methods Clin Dev*. 2018;9:278–287. doi: 10.1016/j.omtm.2018.03.008
33. Wassmer SJ, Carvalho LS, Gyorgy B, Vandenberghe LH, Maguire CA. Exosome-associated AAV2 vector mediates robust gene delivery into the murine retina upon intravitreal injection. *Sci Rep*. 2017;7:45329. doi: 10.1038/srep45329
34. Gyorgy B, Fitzpatrick Z, Crommentuijn MH, Mu D, Maguire CA. Naturally enveloped AAV vectors for shielding neutralizing antibodies and robust gene delivery in vivo. *Biomaterials*. 2014;35:7598–7609. doi: 10.1016/j.biomaterials.2014.05.032
35. Liu B, Li Z, Huang S, Yan B, He S, Chen F, Liang Y. AAV-containing exosomes as a novel vector for improved gene delivery to lung cancer cells. *Front Cell Dev Biol*. 2021;9:707607. doi: 10.3389/fcell.2021.707607
36. Cheng M, Dietz L, Gong Y, Eichler F, Nammour J, Ng C, Grimm D, Maguire CA. Neutralizing antibody evasion and transduction with purified extracellular vesicle-enveloped adeno-associated virus vectors. *Hum Gene Ther*. 2021;32:1457–1470. doi: 10.1089/hum.2021.122
37. Ban JJ, Lee M, Im W, Kim M. Low pH increases the yield of exosome isolation. *Biochem Biophys Res Commun*. 2015;461:76–79. doi: 10.1016/j.bbrc.2015.03.172
38. Kanada M, Bachmann MH, Hardy JW, Frimannson DO, Bronsart L, Wang A, Sylvester MD, Schmidt TL, Kaspar RL, Butte MJ, et al. Differential fates of biomolecules delivered to target cells via extracellular vesicles. *Proc Natl Acad Sci USA*. 2015;112:E1433–E1442. doi: 10.1073/pnas.1418401112
39. Elmore ZC, Patrick Havlik L, Oh DK, Anderson L, Daaboul G, Devlin GW, Vincent HA, Asokan A. The membrane associated accessory protein is an adeno-associated viral egress factor. *Nat Commun*. 2021;12:6239. doi: 10.1038/s41467-021-26485-4
40. Wright JF. AAV empty capsids: for better or for worse? *Mol Ther*. 2014;22:1–2. doi: 10.1038/mt.2013.268
41. Sahoo S, Losordo DW. Exosomes and cardiac repair after myocardial infarction. *Circ Res*. 2014;114:333–344. doi: 10.1161/CIRCRESAHA.114.300639
42. Sahoo S, Klychko E, Thorne T, Misener S, Schultz KM, Millay M, Ito A, Liu T, Kamide C, Agrawal H, et al. Exosomes from human CD34(+) stem cells mediate their proangiogenic paracrine activity. *Circ Res*. 2011;109:724–728. doi: 10.1161/CIRCRESAHA.111.253286
43. Théry C, Witwer KW, Aikawa E, Alcaraz MJ, Anderson JD, Andriantsitohaina R, Antoniou A, Arab T, Archer F, Atkin-Smith GK. Minimal information for studies of extracellular vesicles 2018 (MISEV2018): a position statement of the International Society for Extracellular Vesicles and update of the MISEV2014 guidelines. *J Extracell Vesicles*. 2018;7:1535750. doi: 10.1080/20013078.2018.1535750
44. Boutin S, Monteilhet V, Veron P, Leborgne C, Benveniste O, Montus MF, Masurier C. Prevalence of serum IgG and neutralizing factors against adeno-associated virus (AAV) types 1, 2, 5, 6, 8, and 9 in the healthy population: implications for gene therapy using AAV vectors. *Hum Gene Ther*. 2010;21:704–712. doi: 10.1089/hum.2009.182
45. Gurda BL, DiMattia MA, Miller EB, Bennett A, McKenna R, Weichert WS, Nelson CD, Chen WJ, Muzyczka N, Olson NH, et al. Capsid antibodies to different adeno-associated virus serotypes bind common regions. *J Virol*. 2013;87:9111–9124. doi: 10.1128/JVI.00622-13
46. Gurda BL, Raupp C, Popa-Wagner R, Naumer M, Olson NH, Ng R, McKenna R, Baker TS, Kleinschmidt JA, Agbandje-McKenna M. Mapping a neutralizing epitope onto the capsid of adeno-associated virus serotype 8. *J Virol*. 2012;86:7739–7751. doi: 10.1128/JVI.00218-12
47. Tseng YS, Vliet KV, Rao L, McKenna R, Byrne BJ, Asokan A, Agbandje-McKenna M. Generation and characterization of anti-adeno-associated virus serotype 8 (AAV8) and anti-AAV9 monoclonal antibodies. *J Virol Methods*. 2016;236:105–110. doi: 10.1016/j.jviromet.2016.07.009
48. Peters CW, Maguire CA, Hanlon KS. Delivering AAV to the central nervous and sensory systems. *Trends Pharmacol Sci*. 2021;42:461–474. doi: 10.1016/j.tips.2021.03.004

49. Griciuc A, Federico AN, Natasan J, Forte AM, McGinty D, Nguyen H, Volak A, LeRoy S, Gandhi S, Lerner EP, et al. Gene therapy for Alzheimer's disease targeting CD33 reduces amyloid beta accumulation and neuroinflammation. *Hum Mol Genet*. 2020;29:2920–2935. doi: 10.1093/hmg/ddaa179
50. Ghosh A, Yue Y, Duan D. Viral serotype and the transgene sequence influence overlapping adeno-associated viral (AAV) vector-mediated gene transfer in skeletal muscle. *J Gene Med*. 2006;8:298–305. doi: 10.1002/jgm.835
51. Westhaus A, Cabanes-Creus M, Rybicki A, Baltazar G, Navarro RG, Zhu E, Drouyer M, Knight M, Albu RF, Ng BH, et al. High-throughput in vitro, ex vivo, and in vivo screen of adeno-associated virus vectors based on physical and functional transduction. *Hum Gene Ther*. 2020;31:575–589. doi: 10.1089/hum.2019.264
52. Scallan CD, Jiang H, Liu T, Patarroyo-White S, Sommer JM, Zhou S, Couto LB, Pierce GF. Human immunoglobulin inhibits liver transduction by AAV vectors at low AAV2 neutralizing titers in SCID mice. *Blood*. 2006;107:1810–1817. doi: 10.1182/blood-2005-08-3229
53. Sahoo S, Kariya T, Ishikawa K. Targeted delivery of therapeutic agents to the heart. *Nat Rev Cardiol*. 2021;18:389–399. doi: 10.1038/s41569-020-00499-9
54. Prasad KM, Smith RS, Xu Y, French BA. A single direct injection into the left ventricular wall of an adeno-associated virus 9 (AAV9) vector expressing extracellular superoxide dismutase from the cardiac troponin-T promoter protects mice against myocardial infarction. *J Gene Med*. 2011;13:333–341. doi: 10.1002/jgm.1576
55. Kho C, Lee A, Jeong D, Oh JG, Gorski PA, Fish K, Sanchez R, DeVita RJ, Christensen G, Dahl R, et al. Small-molecule activation of SERCA2a SUMOylation for the treatment of heart failure. *Nat Commun*. 2015;6:7229. doi: 10.1038/ncomms8229
56. Cutler MJ, Wan X, Plummer BN, Liu H, Deschenes I, Laurita KR, Hajjar RJ, Rosenbaum DS. Targeted sarcoplasmic reticulum Ca2+ ATPase 2a gene delivery to restore electrical stability in the failing heart. *Circulation*. 2012;126:2095–2104. doi: 10.1161/CIRCULATIONAHA.111.071480
57. Fargnoli AS, Katz MG, Yarnall C, Isidro A, Petrov M, Steuerwald N, Ghosh S, Richardville KC, Hillesheim R, Williams RD, et al. Cardiac surgical delivery of the sarcoplasmic reticulum calcium ATPase rescues myocytes in ischemic heart failure. *Ann Thorac Surg*. 2013;96:586–595. doi: 10.1016/j.athoracsur.2013.04.021
58. Kranias EG, Hajjar RJ. Modulation of cardiac contractility by the phospholamban/SERCA2a regulatome. *Circ Res*. 2012;110:1646–1660. doi: 10.1161/CIRCRESAHA.111.259754
59. Kho C, Lee A, Jeong D, Oh JG, Chaanine AH, Kizana E, Park WJ, Hajjar RJ. SUMO1-dependent modulation of SERCA2a in heart failure. *Nature*. 2011;477:601–605. doi: 10.1038/nature10407
60. Lipskaia L, Keuylian Z, Blirando K, Mougenot N, Jacquet A, Rouxel C, Sghairi H, Elaib Z, Blaise R, Adnot S, et al. Expression of sarco (endo) plasmic reticulum calcium ATPase (SERCA) system in normal mouse cardiovascular tissues, heart failure and atherosclerosis. *Biochim Biophys Acta*. 2014;1843:2705–2718. doi: 10.1016/j.bbamcr.2014.08.002
61. Kumarswamy R, Lyon AR, Volkmann I, Mills AM, Bretthauer J, Pahuja A, Geers-Knorr C, Kraft T, Hajjar RJ, Macleod KT, et al. SERCA2a gene therapy restores microRNA-1 expression in heart failure via an Akt/FoxO3A-dependent pathway. *Eur Heart J*. 2012;33:1067–1075. doi: 10.1093/eurheartj/ehs043
62. Pleger ST, Shan C, Ksienzyk J, Bekeredjian R, Boekstegers P, Hinkel R, Schinkel S, Leuchs B, Ludwig J, Qiu G, et al. Cardiac AAV9-S100A1 gene therapy rescues post-ischemic heart failure in a preclinical large animal model. *Sci Transl Med*. 2011;3:92ra–9264. doi: 10.1126/scitranslmed.3002097
63. Tabebordbar M, Lagerborg KA, Stanton A, King EM, Ye S, Tellez L, Krunnfusz A, Tavakoli S, Widrick JJ, Messemer KA, et al. Directed evolution of a family of AAV capsid variants enabling potent muscle-directed gene delivery across species. *Cell*. 2021;184:4919–4938.e22. doi: 10.1016/j.cell.2021.08.028
64. Dhungel BP, Bailey CG, Rasko JEJ. Journey to the center of the cell: tracing the path of AAV transduction. *Trends Mol Med*. 2021;27:172–184. doi: 10.1016/j.molmed.2020.09.010
65. Berry GE, Asokan A. Cellular transduction mechanisms of adeno-associated viral vectors. *Curr Opin Virol*. 2016;21:54–60. doi: 10.1016/j.coviro.2016.08.001
66. Riyad JM, Weber T. Intracellular trafficking of adeno-associated virus (AAV) vectors: challenges and future directions. *Gene Ther*. 2021;28:683–696. doi: 10.1038/s41434-021-00243-z
67. Nonnenmacher M, Weber T. Adeno-associated virus 2 infection requires endocytosis through the CLIC/GEEC pathway. *Cell Host Microbe*. 2011;10:563–576. doi: 10.1016/j.chom.2011.10.014
68. Pillay S, Meyer NL, Puschnik AS, Davulcu O, Diep J, Ishikawa Y, Jae LT, Wosen JE, Nagamine CM, Chapman MS, et al. An essential receptor for adeno-associated virus infection. *Nature*. 2016;530:108–112. doi: 10.1038/nature16465
69. Pillay S, Zou W, Cheng F, Puschnik AS, Meyer NL, Ganaie SS, Deng X, Wosen JE, Davulcu O, Yan Z, et al. Adeno-associated virus (AAV) serotypes have distinctive interactions with domains of the cellular AAV receptor. *J Virol*. 2017;91:e00391–e00397. doi: 10.1128/JVI.00391-17
70. Bayer N, Schober D, Prchla E, Murphy RF, Blaas D, Fuchs R. Effect of bafilomycin A1 and nocodazole on endocytic transport in HeLa cells: implications for viral uncoating and infection. *J Virol*. 1998;72:9645–9655. doi: 10.1128/JVI.72.12.9645-9655.1998
71. Vassalli G, Büeler H, Dudler J, von Segesser LK, Kappenberger L. Adeno-associated virus (AAV) vectors achieve prolonged transgene expression in mouse myocardium and arteries in vivo: a comparative study with adenovirus vectors. *Int J Cardiol*. 2003;90:229–238. doi: 10.1016/s0167-5273(02)00554-5
72. Rogers GL, Huang C, Clark RD, Seclén E, Chen H-Y, Cannon PM. Optimization of AAV6 transduction enhances site-specific genome editing of primary human lymphocytes. *Mol Ther Methods Clin Dev*. 2021;23:198–209. doi: 10.1016/j.omtm.2021.09.003
73. Lochrie M, Tatsuno G, Arbetman A, Smith P, Wellman J, Zhou S-z, Pierce G, Colosi P. 130: Characterization of a murine adeno-associated virus (AAV-mo. 1) capsid. *Mol Ther*. 2005;11(suppl 1):S52–S53. doi: 10.1016/j.ymthe.2005.06.135
74. Schmidt M, Katano H, Bossis I, Chiorini JA. Cloning and characterization of a bovine adeno-associated virus. *J Virol*. 2004;78:6509–6516. doi: 10.1128/JVI.78.12.6509-6516.2004
75. Virag JI, Murry CE. Myofibroblast and endothelial cell proliferation during murine myocardial infarct repair. *Am J Pathol*. 2003;163:2433–2440. doi: 10.1016/S0002-9440(10)63598-5
76. Mathieu M, Martin-Jaular L, Lavieu G, Théry C. Specificities of secretion and uptake of exosomes and other extracellular vesicles for cell-to-cell communication. *Nat Cell Biol*. 2019;21:9–17. doi: 10.1038/s41556-018-0250-9
77. Joshi BS, de Beer MA, Giepmans BNG, Zuhorn IS. Endocytosis of extracellular vesicles and release of their cargo from endosomes. *ACS Nano*. 2020;14:4444–4455. doi: 10.1021/acsnano.9b10033
78. Large EE, Silveria MA, Zane GM, Weerakoon O, Chapman MS. Adeno-associated virus (AAV) gene delivery: dissecting molecular interactions upon cell entry. *Viruses*. 2021;13:1336. doi: 10.3390/v13071336
79. Bonsergent E, Grisard E, Buchrieser J, Schwartz O, Théry C, Lavieu GJN. Quantitative characterization of extracellular vesicle uptake and content delivery within mammalian cells. *Nat Commun*. 2021;12:1–11. doi: 10.1038/s41467-021-22126-y
80. Nonnenmacher ME, Cintrat J-C, Gillet D, Weber TJJ. Syntaxin 5-dependent retrograde transport to the trans-Golgi network is required for adeno-associated virus transduction. *J Virol*. 2015;89:1673–1687. doi: 10.1128/JVI.02520-14
81. Gurung S, Perocheau D, Touramanidou L, Baruteau J. The exosome journey: from biogenesis to uptake and intracellular signalling. *Cell Commun Signal*. 2021;19:47. doi: 10.1186/s12964-021-00730-1
82. Dudek AM, Pillay S, Puschnik AS, Nagamine CM, Cheng F, Qiu J, Carette JE, Vandenberghe LH. An alternate route for adeno-associated virus (AAV) entry independent of AAV receptor. *J Virol*. 2018;92:e02213–e02217. doi: 10.1128/jvi.02213-17
83. Kalra H, Adda CG, Liem M, Ang CS, Mechler A, Simpson RJ, Hulett MD, Mathivanan S. Comparative proteomics evaluation of plasma exosome isolation techniques and assessment of the stability of exosomes in normal human blood plasma. *Proteomics*. 2013;13:3354–3364. doi: 10.1002/pmic.201300282
84. Svensson KJ, Christianson HC, Wittrup A, Bourseau-Guilmain E, Lindqvist E, Svensson LM, Mörgelin M, Belting M. Exosome uptake depends on ERK1/2-heat shock protein 27 signaling and lipid Raft-mediated endocytosis negatively regulated by caveolin-1. *J Biol Chem*. 2013;288:17713–17724. doi: 10.1074/jbc.M112.445403
85. Tian T, Zhu YL, Zhou YY, Liang GF, Wang YY, Hu FH, Xiao ZD. Exosome uptake through clathrin-mediated endocytosis and macropinocytosis and mediating miR-21 delivery. *J Biol Chem*. 2014;289:22258–22267. doi: 10.1074/jbc.M114.588046
86. Antimisiaris SG, Mourtas S, Marazioti A. Exosomes and exosome-inspired vesicles for targeted drug delivery. *Pharmaceutics*. 2018;10:218. doi: 10.3390/pharmaceutics10040218
87. Lener T, Gimona M, Aigner L, Borger V, Buzas E, Camussi G, Chaput N, Chatterjee D, Court FA, Del Portillo HA, et al. Applying extracellular vesicles

based therapeutics in clinical trials: an ISEV position paper. *J Extracell Vesicles*. 2015;4:30087. doi: 10.3402/jev.v4.30087
88. Bozoglu T, Lee S, Ziegler T, Jurisch V, Maas S, Baehr A, Hinkel R, Hoenig A, Hariharan A, Kim CI, et al. Endothelial retargeting of AAV9 in vivo. *Adv Sci*. 2022;9:2103867. doi: 10.1002/advs.202103867
89. Dubois NC, Craft AM, Sharma P, Elliott DA, Stanley EG, Elefanty AG, Gramolini A, Keller G. SIRPA is a specific cell-surface marker for isolating cardiomyocytes derived from human pluripotent stem cells. *Nat Biotechnol*. 2011;29:1011–1018. doi: 10.1038/nbt.2005
90. Orlowski A, Katz MG, Gubara SM, Fargnoli AS, Fish KM, Weber T. Successful transduction with AAV vectors after selective depletion of anti-AAV antibodies by immunoadsorption. *Mol Ther Methods Clin Dev*. 2020;16:192–203. doi: 10.1016/j.omtm.2020.01.004
91. Prasad KM, Xu Y, Yang Z, Acton ST, French BA. Robust cardiomyocyte-specific gene expression following systemic injection of AAV: in vivo gene delivery follows a Poisson distribution. *Gene Ther*. 2011;18:43–52. doi: 10.1038/gt.2010.105
92. Kawase Y, Ly HQ, Prunier F, Lebeche D, Shi Y, Jin H, Hadri L, Yoneyama R, Hoshino K, Takewa Y, et al. Reversal of cardiac dysfunction after long-term expression of SERCA2a by gene transfer in a pre-clinical model of heart failure. *J Am Coll Cardiol*. 2008;51:1112–1119. doi: 10.1016/j.jacc.2007.12.014
93. Kohlbrenner E, Weber T. Production and characterization of vectors based on the cardiotropic AAV serotype 9. In: *Cardiac Gene Therapy*. Springer; 2017:91–107.
94. Zeltner N, Kohlbrenner E, Clément N, Weber T, Linden RM. Near-perfect infectivity of wild-type AAV as benchmark for infectivity of recombinant AAV vectors. *Gene Ther*. 2010;17:872–879. doi: 10.1038/gt.2010.27
95. Chen J, Hammoudi N, Benard L, Ceholski DK, Zhang S, Lebeche D, Hajjar RJ. The probability of inconstancy in assessment of cardiac function post-myocardial infarction in mice. *Cardiovasc Pharm Open Access*. 2016;5:195. doi: 10.4172/2329-6607.1000195
96. Chen J, Tung CH, Allport JR, Chen S, Weissleder R, Huang PL. Near-infrared fluorescent imaging of matrix metalloproteinase activity after myocardial infarction. *Circulation*. 2005;111:1800–1805. doi: 10.1161/01.CIR.0000160936.91849.9F
97. Welsh JA, Van Der Pol E, Arkesteijn GJA, Bremer M, Brisson A, Coumans F, Dignat-George F, Duggan E, Ghiran I, Giebel B, et al. MIFlowCyt-EV: a framework for standardized reporting of extracellular vesicle flow cytometry experiments. *J Extracell Vesicles*. 2020;9:1713526–1713526. doi: 10.1080/20013078.2020.1713526
98. Ishikawa K, Fish KM, Tilemann L, Rapti K, Aguero J, Santos-Gallego CG, Lee A, Karakikes I, Xie C, Akar FG, et al. Cardiac I-1c overexpression with reengineered AAV improves cardiac function in swine ischemic heart failure. *Mol Ther*. 2014;22:2038–2045. doi: 10.1038/mt.2014.127
99. Andrews S. FastQC: a quality control tool for high throughput sequence data. Babraham Bioinformatics, Babraham Institute. 2010. Accessed May 1, 2021. http://www.bioinformatics.babraham.ac.uk/projects/fastqc
100. Bolger AM, Lohse M, Usadel B. Trimmomatic: a flexible trimmer for Illumina sequence data. *Bioinformatics*. 2014;30:2114–2120. doi: 10.1093/bioinformatics/btu170
101. Langmead B, Trapnell C, Pop M, Salzberg SL. Ultrafast and memory-efficient alignment of short DNA sequences to the human genome. *Genome Biol*. 2009;10:R25. doi: 10.1186/gb-2009-10-3-r25
102. Liao Y, Smyth GK, Shi W. featureCounts: an efficient general purpose program for assigning sequence reads to genomic features. *Bioinformatics*. 2014;30:923–930. doi: 10.1093/bioinformatics/btt656
103. R Core Team (2018). A language and environment for statistical computing. R Foundation for Statistical Computing. Accessed May 1, 2019. https://www.R-project.org
104. Hadley W. *ggplot2: Elegant graphics for data analysis*. Springer; 2009:VIII, 213.
105. Robinson MD, Oshlack A. A scaling normalization method for differential expression analysis of RNA-seq data. *Genome Biol*. 2010;11:R25. doi: 10.1186/gb-2010-11-3-r25
106. Bates D, Mächler M, Bolker B, Walker S. Fitting linear mixed-effects models using lme4. *J Stat Softw*. 2015;67:1–48. doi: 10.18637/jss.v067.i01
107. Benjamini Y, Hochberg Y. Controlling the false discovery rate: a practical and powerful approach to multiple testing. *J R Stat Soc Series B (Methodol)*. 1995;57:289–300. doi: 10.1111/j.2517-6161.1995.tb02031.x